SERI/PR-8254-1-T2

AMORPHOUS THIN FILMS FOR SOLAR-CELL APPLICATIONS

Quarterly Report No. 2 for December 11, 1979—March 10, 1980

By
D. E. Carlson
R. S. Crandall
J. Dresner
B. Goldstein
J. J. Hanak
A. R. Moore
J. I. Pankove
H. A. Weakliem

March 1980

Work Performed Under Contract No. AC02-77CH00178

RCA Laboratories
Princeton, New Jersey

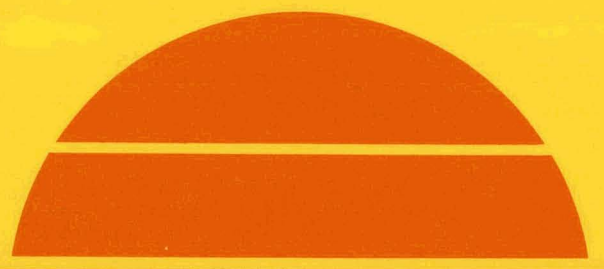

U.S. Department of Energy

Solar Energy

DISCLAIMER

DISCLAIMER

Available from the National Technical Information Service, U. S. Department of Commerce, Springfield, Virginia 22161.

Price: Paper Copy $8.00
Microfiche $3.50

SERI/PR-8254-1-T2
Distribution Category UC-63e

AMORPHOUS THIN FILMS FOR SOLAR-CELL APPLICATIONS

Quarterly Report No. 2

March 1980

D. E. Carlson, R. S. Crandall, J. Dresner,
B. Goldstein, J. J. Hanak, A. R. Moore,
J. I. Pankove, and H. A. Weakliem

RCA Laboratories
Princeton, New Jersey 08540

Prepared Under Subcontract No. XJ-9-8254
for the

Solar Energy Research Institute
A Division of Midwest Research Institute
1536 Cole Boulevard
Golden, Colorado 80401

THIS PAGE

WAS INTENTIONALLY

LEFT BLANK

PREFACE

This Quarterly Report covers the work performed by the Display and Energy Systems Research Laboratory of RCA Laboratories, Princeton, New Jersey, for the period 11 December 1979 to 10 March 1980 under Contract No. XJ-9-8254. The Laboratory Director is B. F Williams; D. E. Carlson is the Group Head and Project Scientist. The staff members and associate staff personnel who have contributed to the report, and their areas of specialization, are listed below.

D. E. Carlson R. W. Smith	dc Deposition of a-Si:H
*R. S. Crandall B. E. Tompkins	Photoconductivy and Transport
*J. Dresner	Hall Effect
*B. Goldstein D. J. Szostak	Surface Studies
†J. J. Hanak J. P. Pellicane V. Korsun	rf Deposition of a-Si:H; Structures
*A. R. Moore G. R. Latham	Photoelectromagnetic Effect
†J. I. Pankove J. E. Berkeyheiser	Photoluminescence
*H. A. Weakliem A. V. Cafiero	rf Magnetron Deposition of a-Si:H, Mass Spectroscopy

*Member of Technical Staff.
†Fellow.

THIS PAGE

WAS INTENTIONALLY

LEFT BLANK

SUMMARY

Measurements of both primary and secondary photocurrents for photon energies between 0.58 and 2.0 eV in a-Si:H solar-cell structures have been used to provide information about the density of states above the valence band as well as show that holes are mobile deep in the bandgap. Measurements of the response time of the secondary photocurrent as well as its magnitude have been used to determine the majority carrier drift mobility for excitation energies above and below the bandgap. The drift mobility is independent of excitation energy, indicating that the majority carriers are excited to the same states, irrespective of the excitation energy.

Deposition studies in the dc proximity system have shown that the conductivity and photoconductivity of doped films (both boron- and phosphorus-doped) increase with substrate temperature (up to the maximum temperature studied, ~350°C.)

Mass spectroscopy studies have shown that the larger $Si_xH_y^+$ clusters are favored by operating rf discharges at low rf powers and high pressures. Moreover, infrared absorption spectra show that the larger the $Si_xH_y^+$ cluster in the discharge, the smaller the concentration of SiH_2 and $(SiH_2)_n$ groups in the a-Si:H film. The positive ion spectrum of a discharge in SiH_4 + 1% B_2H_6 shows that the concentration of $B_2H_5^+$ is comparable to that of the main silane ion, SiH_3^+.

We find that a better fit to the photoluminescence data can be obtained by plotting the luminescence efficiency as a function of $\exp(-T/T_o)$ rather than as a function of $\exp(E_o/kT)$. However, the physical meaning of this observation is not clear.

The Hall mobility is roughly constant below 360 K but exhibits a thermal activation energy of ~0.13 eV at higher temperatures. These observations rule out simple extended-state transport as the conduction mechanism.

The photoelectromagnetic effect has been used to estimate the hole lifetime ($\sim 3.4 \times 10^{-7}$ s) in undoped a-Si:H; the electron lifetime is $\sim 1.7 \times 10^{-6}$ s.

An a-Si:H monolithic solar panel consisting of 16 cells in series has been fabricated on a 4" x 4" glass substrate (63 cm^2 of active area), and the panel exhibits a conversion efficiency of 3.6%.

A preliminary optimization of p-i-n structures illuminated through the n-layer indicates that the thickness of the n-layer should be $\lesssim$5 nm and that of the i-layer, $\sim$0.6 μm for devices made in an rf capacitive discharge. An efficiency of 3.6% was obtained in these experiments. The best cells produced in an rf magnetron discharge exhibited efficiencies of $\lesssim$2.5%.

In another series of experiments, the thicknesses and doping levels of p-i-n cells made in a dc(P) discharge were optimized. The best cell made in these experiments had an efficiency of 5.3% with an area of 1.19 cm^2.

Surface photovoltage profiling has been used to determine the relative contributions of various interfaces and layers to the built-in potential of p-i-n cells. The ITO/p-layer interface in an ITO/p-i-n cell apparently contributes $\sim$200 mV to the built-in potential.

TABLE OF CONTENTS

TABLE OF CONTENTS (Continued)

LIST OF ILLUSTRATIONS

LIST OF ILLUSTRATIONS (Continued)

LIST OF ILLUSTRATIONS (Continued)

LIST OF ILLUSTRATIONS (Continued)

LIST OF TABLES

SECTION 1.0

INTRODUCTION

A review of the history of hydrogenated amorphous silicon (a-Si:H) and the a-Si:H solar cell can be found in Refs. 1 and 2. The present research program involves five tasks: theoretical modeling, deposition and doping studies, experimental methods for the characterization of a-Si:H, formation of solar-cell structures, and theoretical and experimental evaluation of solar-cell parameters.

In a separate program, researchers at RCA Laboratories are developing the technology to fabricate large-area ($\sim$40 cm^2) a-Si:H solar cells. This program has the objective of developing low-cost, large-area a-Si:H solar panels.

---

1. D. E. Carlson, R. S. Crandall, B. Goldstein, J. J. Hanak, A. R. Moore, J. I. Pankove, and D. L. Staebler, Final Report, SAN-1286-8, prepared for Department of Energy under Contract No. EY-C-03-1286, Oct. 1978.
2. D. E. Carlson, I. Balberg, R. S. Crandall, B. Goldstein, J. J. Hanak, J. I. Pankove, D. L. Staebler, H. A. Weakliem, and R. Williams, Final Report, ET/21074-4, prepared for Department of Energy under Contract No. AC03-78-ET-21074, Feb. 1980.

SECTION 2.0

THEORETICAL MODELING - PHOTOCONDUCTIVITY AND TRANSPORT IN a-Si:H

2.1 INTRODUCTION

Photocurrent measurements on insulators and semiconductors have been frequently used to detect defects that are in such low concentration that they are undetectable by optical transmission measurements. Some of the early work has been reviewed by Moss [3]. In hydrogenated amorphous silicon (a-Si:H), photocurrent measurements have been made using below-bandgap excitation to gain information about the bandtail states [4-10]. In general, the measurements show a broad region of photocurrent extending well below the optical absorption edge with a threshold at about 0.6 eV. Some of the measurements [5] show the photoconductivity decreasing monotonically with decreasing photon energy, whereas others show a shoulder in the spectral dependence [4] or even definite structure [6-9]. The authors [4-9] conclude that the photocurrent is proportional to the absorption coefficient (α) and hence, gives a measure of the density of bandtail states. However, this conclusion is not well supported because the photocurrent, besides being proportional to α, is proportional to the product of the mobility (μ) and the photocarrier lifetime (τ). Even though it is usually assumed that the $\mu\tau$ product is independent of the excitation energy, there is evidence [10] that this is not the case in a-Si:H. Nevertheless, by making photoconductivity measurements under special conditions, it is possible to separate effects due to the spectral dependence of α from those due to the spectral dependence of the $\mu\tau$ product [10]. Then one can

3. T. S. Moss, Photoconductivity in the Elements (Academic Press, New York, 1952).
4. P. G. LeComber, A. Madan, and W. E. Spear, in P. G. Lecomber and J. Mort, (eds.) Electronic and Structural Properties of Amorphous Semiconductors (Academic Press, New York, 1973) p. 373.
5. T. Suzuki, M. Hirose, S. Ogose, and Y. Osaka, Phys. Status Solidi A 42, 337 (1977).
6. P. J. Zanzucchi, C. R. Wronski, and D. E. Carlson, J. Appl. Phys. 48, 5227 (1977).
7. D. A. Anderson, G. Moddel, R. W. Collins, and W. Paul, paper presented at 8th Int. Liquid and Amorphous Semiconductors, Cambridge, MA (1979).
8. J. I. Pankove, F. J. Pollack, and C. Schnabolk, ibid.
9. G. D. Cody, B. Abeles, and C. R. Wronski, ibid.
10. R. S. Crandall, J. Non-Cryst. Solids 35 & 36, 38 (1980).

draw reliable conclusions about the spectral dependence of α. It is this approach that will be followed in this section.

There are actually two types of photocurrent that can be measured. They have been referred to in the literature [3,11] as primary and secondary photocurrents. They are distinguished by the details of the measurement. A primary photocurrent (PPC) is measured if the contacts to the photoconductor are blocking. This is the type of current usually measured in wide bandgap insulators such as the alkali halides. A secondary photocurrent (SPC) is measured if the contacts to the photoconductor are ohmic. A SPC has the property that more than one charge carrier can flow through the external circuit for each absorbed photon. In other words it exhibits gain (g). The PPC admits, at most, one electron in the external circuit per absorbed photon. In fact, one can use this property to measure the number of absorbed photons. This measurement combined with a measurement of the SPC then determines the $\mu\tau$ product. The most convenient structure to measure both PPC and SPC is a thin-film solar cell in which the electric field extends throughout the thin film. This is because the reverse-bias photocurrent is primary, whereas for a forward bias greater than the flatband voltage the photocurrent is secondary.

This work describes measurements of the spectral dependence of both primary and secondary photocurrents in a-Si:H solar cells. The absorption coefficient is calculated from the primary photocurrent. This gives the first measurement of α for the weakly absorbing gap states. Transient secondary photocurrent measurements are used to determine the drift mobility of the majority carriers, indicating that photon absorption by gap states produces electrons in the same states as absorption by band states. This result leads to the conclusion that holes are mobile gap states far above the valence band.

2.2 MODEL

2.2.1 dc Photocurrent

As the model for the a-Si:H solar cell we take the idealized structure depicted by the potential energy diagram shown in Fig. 2-1. An insulating film of a-Si:H is sandwiched between a Schottky-barrier contact (M_1) and a region of heavily

11. A. Rose, RCA Review 12, 362 (1951).

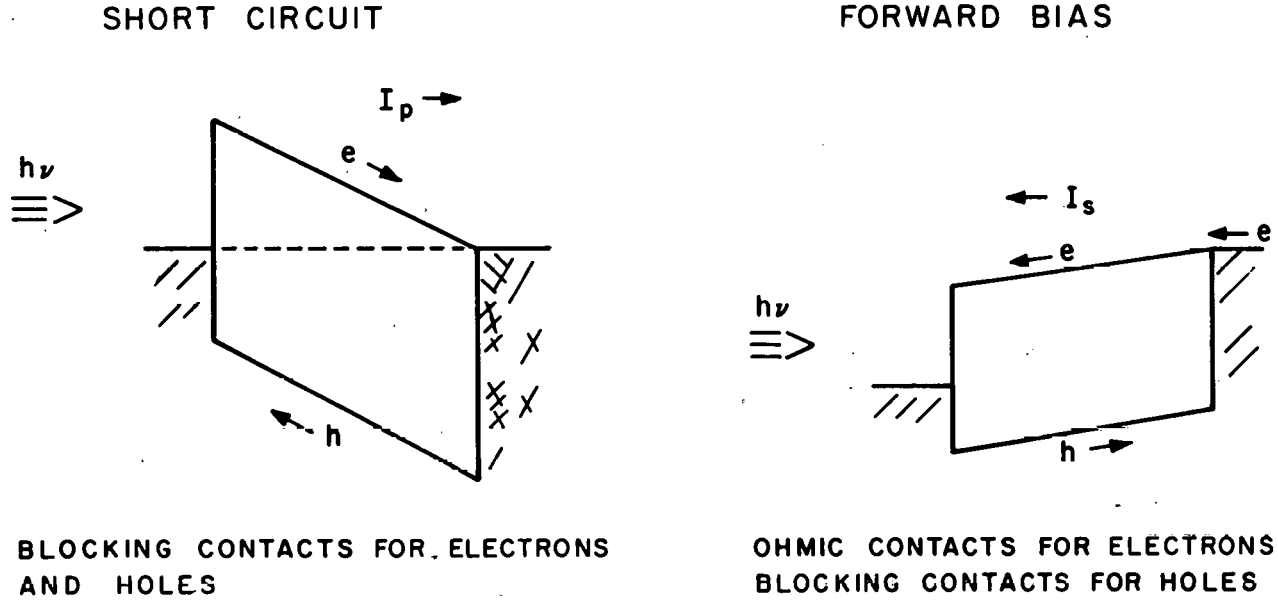

Figure 2-1. SCHEMATIC OF IDEALIZED POTENTIAL ENERGY DIAGRAM FOR AN a-Si:H SCHOTTKY-BARRIER SOLAR CELL

doped a-Si:H on a metal contact. We represent this by M_2. The electric field, for the short-circuit configuration in Fig. 2-1(a), is shown to be uniform in the insulating film. This is actually a good representation of the best thin-film solar-cell structures [12]. Light passes through the semitransparent contact M_1 exciting electron-hole pairs in the a-Si:H. In this structure both contacts M_1 and M_2 are blocking so that the reverse-bias current is primary. At low fields the PPC varies linearly with field [11,13]. However, at high fields it saturates at the value.

$$J_p = eN_A \tag{2-1}$$

where N_A is the number of ionized electron-hole pairs per cm^2/s. Under these conditions the electron and hole traverse the film without significant recombination. Also, a saturated PPC indicates that geminate recombination of the excited electron-hole pair is not important [14]. The current J_p is due to an equal number of electrons and holes. With the assumption that each absorbed

12. R. Williams and R. S. Crandall, RCA Review 40, 371 (1979).
13. K. Hecht, Z. Phys. 77, 235 (1932).
14. R. S. Crandall, R. Williams, and B. E. Tompkins, J. Appl. Phys. 50, 5506 (1979). R. S. Crandall, Appl. Phys. Lett.

photon produces an ionized electron-hole pair, J_p is a measure of the absorption coefficient. In what follows, when the PPC is referred to, we mean its saturated value given by Eq. (2-1).

The saturated value of the reverse-bias PPC determines N_A which can be related to the optical absorption coefficient by

$$N_A = N_i \, [1-\rho_2 \exp(-2\alpha\ell) - (1-\rho_2) \exp(-\alpha\ell)] \, [1-\rho_1] \qquad (2\text{-}2)$$

where N_1 is the density of incident photons, ρ_2 the reflectivity of the back contact (M_2), ρ_1 the reflectivity of the Schottky-barrier contact (M_1), and ℓ the thickness of the insulating layer.

To measure the SPC in a thin-film solar cell it must be biased past the flat-band condition as shown in Fig. 2-1(b). In this configuration M_2 becomes an injecting contact for electrons. Contact M_1, under these conditions, remains a blocking contact for holes. Therefore, the photocurrent in this configuration is a SPC for electrons and a PPC for holes. Because the secondary current exhibits photoconductive gain, the electron current will dominate under most conditions. The SPC can be written as

$$J_s = eN_A \frac{\tau}{\ell} \mu E = eN_A g \qquad (2\text{-}3)$$

where E is the electric field and ℓ the sample thickness. The gain (g) is the ratio of lifetime τ to transit time ($\ell/\mu E$). Usually, N_A is determined by measuring the reflectivity, absorption coefficient, and by assuming that the quantum efficiency for free-carrier production is unity. However, it is usually difficult to reliably determine these parameters, and the assumption of unity quantum efficiency is not always justified [14]. Nevertheless, in solar-cell structures, N_A can be readily determined from the saturated PPC, by the use of (2-1).

2.2.2 Transient Photocurrent

Additional information can be obtained by measuring the transient SPC. In principle, one can measure the majority carrier lifetime this way and then, using Eq. (2-3), determine the mobility. However, the characteristic time in a transient photocurrent measurement is the response time (τ_R) which, in practice, is longer than τ due to trapping effects [11]. In this case the

resulting mobilty will be a trap-dominated drift mobility (μ_D). The response time is defined by

$$\frac{1}{\tau_R} = - \left. \frac{d\ell n(J_S)}{dt} \right|_{t = 0} \tag{2-4}$$

The response time, so defined, is that for photocarriers in the steady state [15]. One can then measure the $\mu\tau$ product by the use of different photon energies for excitations that put electrons and holes into states in the conduction and valence bands as well as in tail states. Then, from a measurement of τ_R one can determine μ_D from the $\mu\tau$ product by the use of

$$\mu_D \tau_R = \mu\tau \tag{2-5}$$

2.3 EXPERIMENTAL DETAILS

The solar-cell structures are conventional Schottky-barrier cells [16]. The a-Si:H was produced by either rf or dc glow-discharge decomposition of silane on heated substrates of either metal-coated glass or stainless steel. First, a thin phosphorus-doped layer of a-Si:H was grown on the substrate. This was followed by a thick, undoped or lightly doped layer of a-Si:H. The Schottky barrier was made by electron-beam evaporation of either platinum or indium-tin-oxide (ITO). The optical excitation source was a quartz iodine-tungsten lamp whose output was dispersed by 1/2 meter Jarrel Ash grating monochromator. Suitable filters were mounted at the output to cut out unwanted orders as well as stray light. The light was chopped at low frequency. The primary photocurrent was measured with a phase-sensitive detector. Because the response time of the secondary photocurrent can be longer than one second, an electrometer was used to measure this current. Measurements of the transient photocurrent were made with either pulsed solid-state lasers or a cw He-Ne laser whose light output was mechanically interrupted. To obtain a fast response the laser beam was focused onto the blade of a copper wheel. This gaves a system response of better than 300 ns. The pulsed lasers, which operated at

15. T. D. Moustakas and K. Weiser, Phys. Rev. B12, 2448 (1975).
16. C. R. Wronski, D. E. Carlson, and R. E. Daniel, Appl. Phys. Lett. 29, 602 (1976).

1.49 and 0.99 eV, respectively, had response times faster than 1 ns. Measurements at different temperatures were made in a conventional liquid nitrogen Dewar.

2.4 EXPERIMENTAL RESULTS

2.4.1 dc Photocurrent

In Fig. 2-2 the photocurrent is plotted vs applied voltage. The measurement temperature was 250 K and the excitation wavelength was 0.83 μm. The general features of this data were also observed at other wavelengths. The data are similar for excitation above or below the bandgap. In the figure, positive currents are primary photocurrents; negative secondary. The voltage V_F is the flatband voltage which is determined experimentally by the point of which the photocurrent changes sign. At this voltage the current changes from primary to secondary. The fact that there is photoconductive gain is evident from the result that the current for a given voltage relative to V_F is higher for the SPC than for the PPC. The important feature of this data is that the primary photocurrent saturates in reverse bias. This means that at large reverse bias all the excited electron-hole pairs are collected. In other words, both electrons and holes are transported through the a-Si:H film without significant recombination. In a-Si:H solar cells the collection region is the region of high electric field or depletion region [17]. The minority carrier diffusion length is too short to give appreciable photocurrents for carriers produced outside the depletion region [18]. For the data in Fig. 2-2 the film is fully depleted so that the collection length is equal to the film thickness, 0.6 μm. The depletion width was determined from capacitance measurements under illumination [12]. The best evidence that the depletion width equals the sample thickness is that the photocurrent saturates in reverse bias. The decrease in photocurrent at small reverse bias and in forward bias is mainly caused by electron-hole recombination in the insulating layer. The saturation of the photocurrent in reverse bias also indicates that geminate recombination [14] is not important at these high fields.

17. C. R. Wronski, D. F. Carlson, R. E. Daniel, and A. R. Triano, IEDM Technical Digest 75 (1976).
18. D. L. Staebler, Paper Presented at 8th Int. Conf. Liquid and Amorphous Semiconductors, Cambridge, MA, 1979.

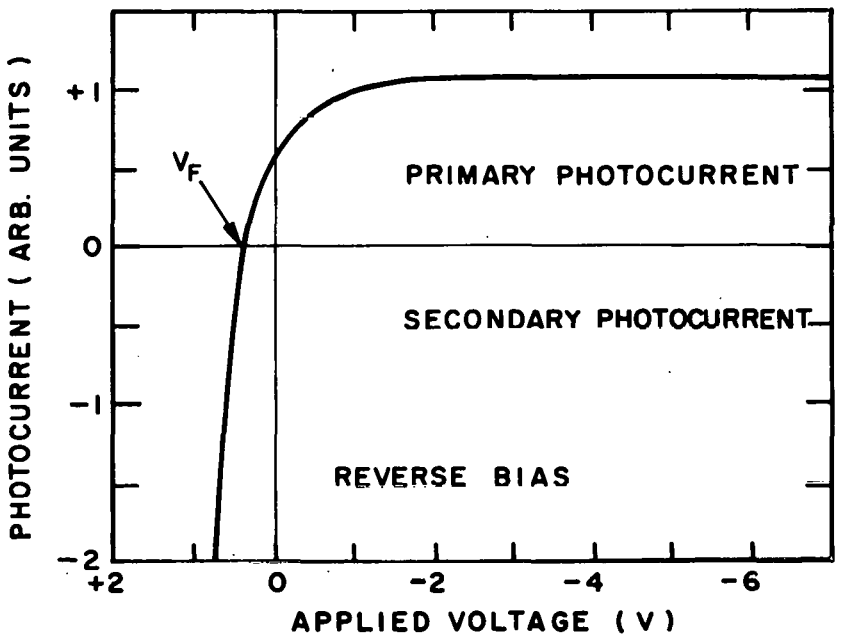

Figure 2-2. PHOTOCURRENT vs VOLTAGE APPLIED TO A SCHOTTKY-BARRIER a-Si:H SOLAR CELL. THE POLARITY IS THAT OF THE Pt BARRIER CONTACT. THE PHOTON ENERGY IS 1.49 eV AND THE TEMPERATURE 250 K. THE UNDOPED FILM THICKNESS IS 0.6 μm

Results of measurements of the spectral dependence of the photocurrent is shown in Fig. 2-3. Both the PPC and SPC, as well as the gain, are plotted as a function of photon energy. The PPC was measured at a reverse bias greater than 2 V and the SPC was measured at large enough forward bias to ensure that the current was ohmic. The PPC, labeled J_p exhibits a monotonic decrease with decreasing photon energy. There is no significant structure, even at the absorption edge, which is about 1.65 eV. The absorption edge was determined in the usual way [19] by plotting $(\alpha h\upsilon)^{1/2}$ vs photon energy ($h\upsilon$), and taking the extrapolated intercept on the energy axis as E_g. The secondary photocurrent (SPC), on the other hand, shows a sizable peak in the neighborhood of 1.1 eV. Because this structure does not appear in the PPC, it must be due to variations in the gain rather than the absorption coefficient. This is shown by the spectral dependence of g in Fig. 2-3. This type of spectral variation is observed in other films prepared by either dc or rf discharge.

19. J. Tauc, Mater. Res. Bull. 5, 721 (1970).

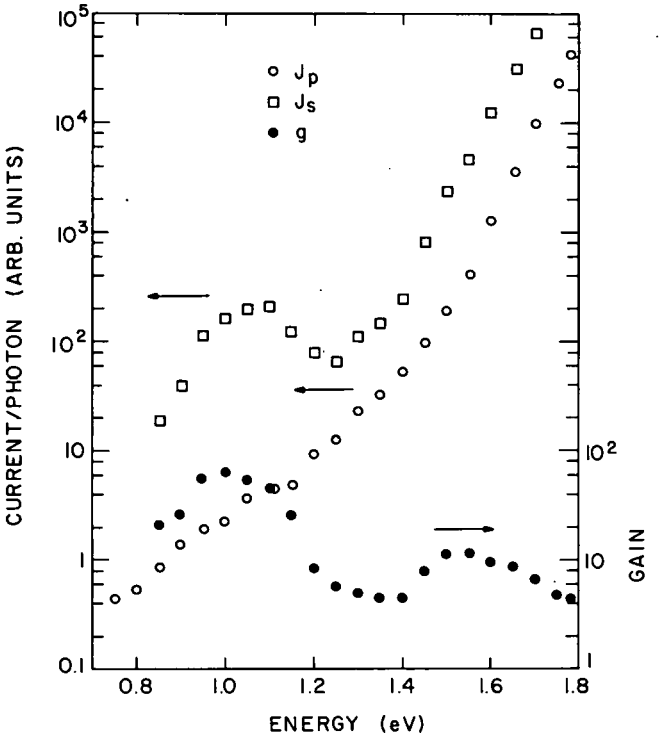

Figure 2-3. SPECTRAL DEPENDENCE OF THE PRIMARY (J_p) AND SECONDARY J_s PHOTOCURRENTS MEASURED ON AN a-Si:H SCHOTTKY-BARRIER SOLAR-CELL STRUCTURE AT ROOM TEMPERATURE. THE UNDOPED FILM THICKNESS IS 0.48 μm. THE GAIN g IS THE RATIO OF J_s TO J_p. THE SCHOTTKY-BARRIER MATERIAL IS ITO. TO CONVERT J_p TO α MULTIPLY BY 0.08 cm^{-1}

However, this peak is not always at the same energy, and in some cases, a shoulder instead of a distinct maximum is observed. It is this general type of spectral dependence of J_s that is often reported [3-9]. If one were to conclude that J_s represents the spectral dependence of N_A and, hence, is a measure of the gap-state density, the conclusion would be that there is peak in the gap-state density. Clearly, this conclusion would be incorrect. This conclusion has been reached by various authors [7-9].

The data for the PPC in Fig. 2-3 can be converted to an optical absorption coefficient by multiplying J_p by 0.08 cm^{-1}. Because of uncertainties in measuring ℓ, ρ_1, and ρ_2, the values of α are probably only good to about 20%.

Absorption coefficient data for a-Si:H doped with different concentrations of phosphorus are shown in Fig. 2-4. Since the solar-cell structures were made on highly reflecting substrates, interference fringes are apparent in the

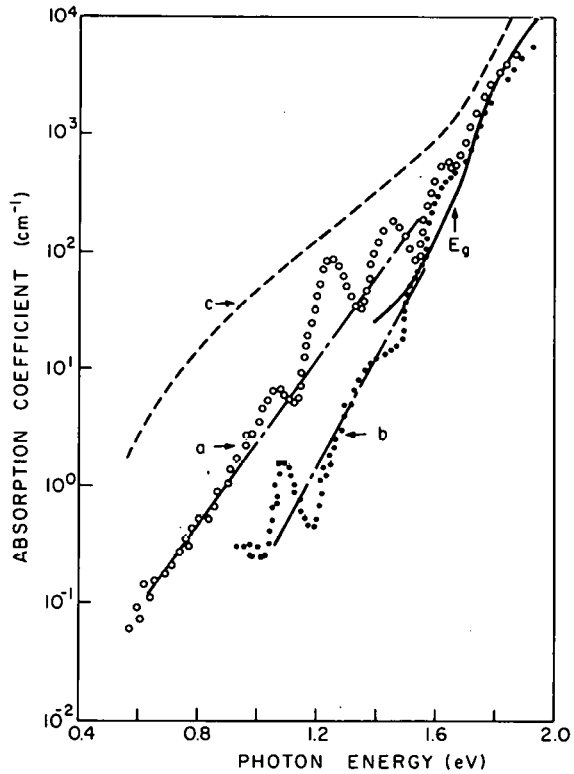

Figure 2-4. THE SOLID CURVE IS THE ABSORPTION COEFFICIENT MEASURED ON A 6.6-μm UNDOPED FILM. CURVE a IS α DETERMINED BY PHOTOVOLTAIC EFFECT ON A 0.5-μm DOPED FILM; CURVE b ON A 0.6-μm-UNDOPED FILM. CURVE c ON A 0.6-μm PHOSPHORUS DOPED FILM. E_g IS THE OPTICAL GAP. THE BARRIER METAL IS PLATINUM

figure. The front surfaces of the cells were given an antireflection coating whose properties change significantly in the infrared regions of the spectrum. Therefore, the fringe amplitude is quite wavelength-dependent. Along with the three curves labeled a, b, and c, which were obtained from PPC measurements, is the solid curve which was obtained from transmission measurements on a 6.6-μm-thick undoped a-Si:H film grown under the same conditions as the insulating layer in the solar-cell structure used to obtain curve b. The absorption coefficient determined from the PPC measurements is seen to be in good agreement with that obtained from optical transmission.

The increase in bandtail absorption with increasing phosphorus content in the film is evident from a comparison of curves b, a, and c. Curve b is for an undoped film which contains less than 1 ppm of phosphorus. Curve a contains about 200 ppm, and curve c contains 2000 ppm of phosphorus. A comparison of

curves a and c indicates that the absorption at low energy scales roughly with phosphorus content.

The photocurrent data in Figs. 2-3 and 2-4 were obtained at room temperature. However, the PPC data show little temperature dependence. This is shown in Fig. 2-5 where the PPC measured at photon energies above and below the absorption edge is plotted as a function of temperature. If the current were temperature-activated, then the activation energy would be very low, between 0.01 and 0.02 eV, depending on photon energy. This is in contrast to the SPC, which shows a much stronger temperature dependence [4,20].

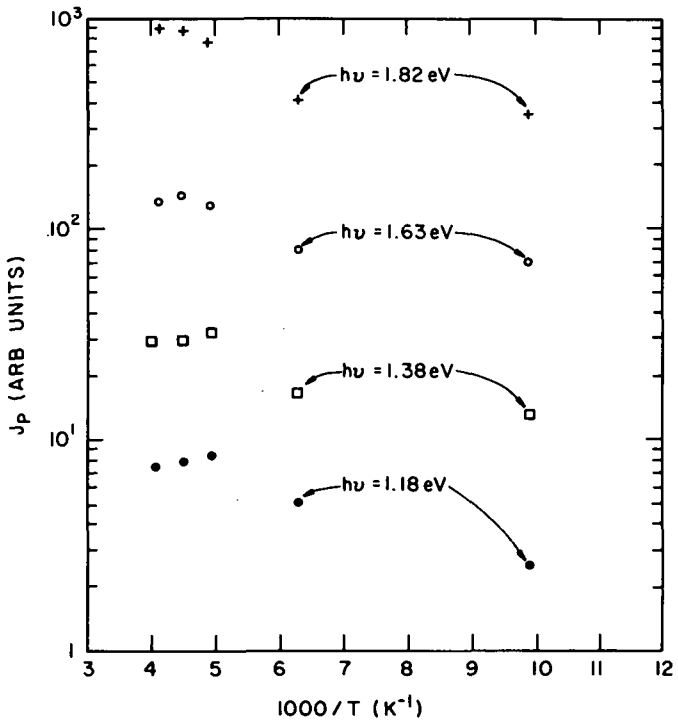

Figure 2-5. TEMPERATURE DEPENDENCE OF THE PPC IN AN a-Si:H SOLAR CELL. SAME CELL AS CURVE b IN FIG. 2-4

Measurements of the PPC on similiarly prepared solar-cell structure which use either platinum or ITO Schottky-barrier contacts give the same spectral response, within experimental error. Therefore, we conclude that the photoconductive process dominates over contact effects such as photoemission.

20. W. Fuhs, M. Milleville, and J. Stuke, Phys. Status Solidi (B) 89, 495 (1978).

2.4.2 Transient Photocurrent

Typical transient SPC data are shown in Fig. 2-6. The current increases linearly with time at short times and then saturates at the dc value. The response time (τ_R), as defined by Eq. (2-4) is the difference between t_1 and t_0, where t_1 is found by extrapolating a line drawn tangent to the initial portion of the current decay. The response time depends somewhat on sample and excitation wavelength. The drift mobility is obtained from this data by combining τ_R with the $\mu\tau$ product, determined from the steady-state SPC, using Eq. (2-5).

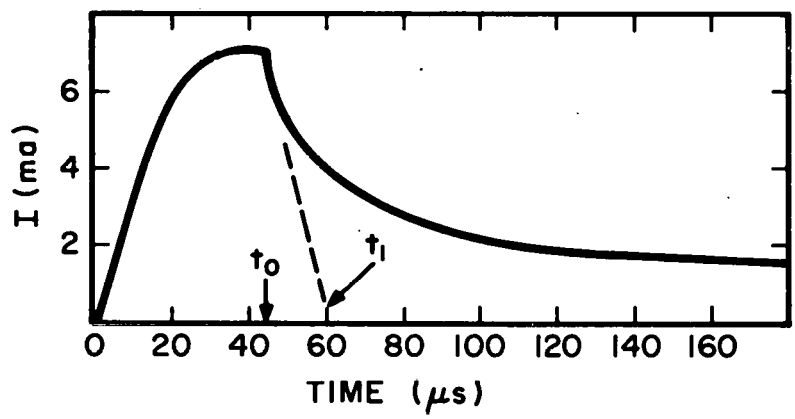

Figure 2-6. TRANSIENT SECONDARY PHOTOCURRENT MEASURED AT ROOM TEMPERATURE USING 0.99-eV EXCITATION

In Fig. 2-7 the drift mobility is plotted vs the voltage relative to the flat-band voltage. The high voltage values of μ_D are the most reliable. At low voltage the number of free electron-hole pairs can be reduced by geminate recombination [14]. Since the value of N_A used in Eq. (2-3) to determine the $\mu\tau$ product was measured at high reverse bias, this effect is not included. Whenever the drift mobility is referred to, it will be the saturated value obtained at high V_A.

The use of different photon energies enables one to then measure the $\mu\tau$ product for excitations that put electrons and holes into states in the conduction and valence bands as well as in tail states. Then, from a measurement of τ_R , μ_D can be determined from the $\mu\tau$ product. Results similar to those in Fig. 2-6

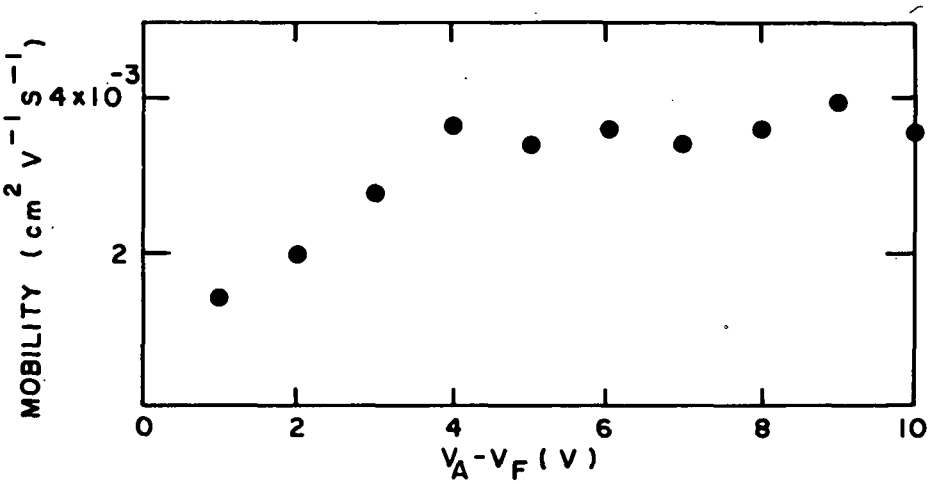

Figure 2-7. DRIFT MOBILITY vs FORWARD-BIAS VOLTAGE ACROSS THE UNDOPED a-Si:H FILM. V_A-V_F IS APPLIED VOLTAGE MINUS FLATBAND VOLTAGE. THE TEMPERATURE IS 264 K AND THE PHOTON ENERGY IS 1.49 eV

were obtained by using other excitation energies. They are shown in Table 2-1 for three different energies of laser light. The excitation energy of 1.99 eV is above the optical bandgap of 1.65 eV, whereas, 1.49 and 0.99 eV are well below the bandgap. The surprising result is that μ_D is virtually independent of excitation energy. The conclusion to be drawn from this result is that the majority carriers, assumed electrons, are ending up in the same state or group of states, irrespective of the excitation energy.

TABLE 2-1. TRANSPORT PARAMETERS MEASURED AT ROOM TEMPERATURE ON UNDOPED a-Si:H. I_{sc} IS THE SHORT-CIRCUIT CURRENT

Photon Energy (eV)	τ_R (μs)	μ_D ($cm^2V^{-1}S^{-1}$)	I_{sc}(A)
1.99	6 + 1	$(7 \pm 2)\times10^{-3}$	7.5×10^{-4}
1.49	7 ± 1	$(6 \pm 2)\times10^{-3}$	2×10^{-4}
0.99	300 ± 50	$(8 \pm 5)\times10^{-3}$	1.6×10^{-6}

Additional support to this idea is given by the temperature dependence of μ_D shown in Fig. 2-8. The activation energy (ΔE = 0.12 eV) is in reasonable

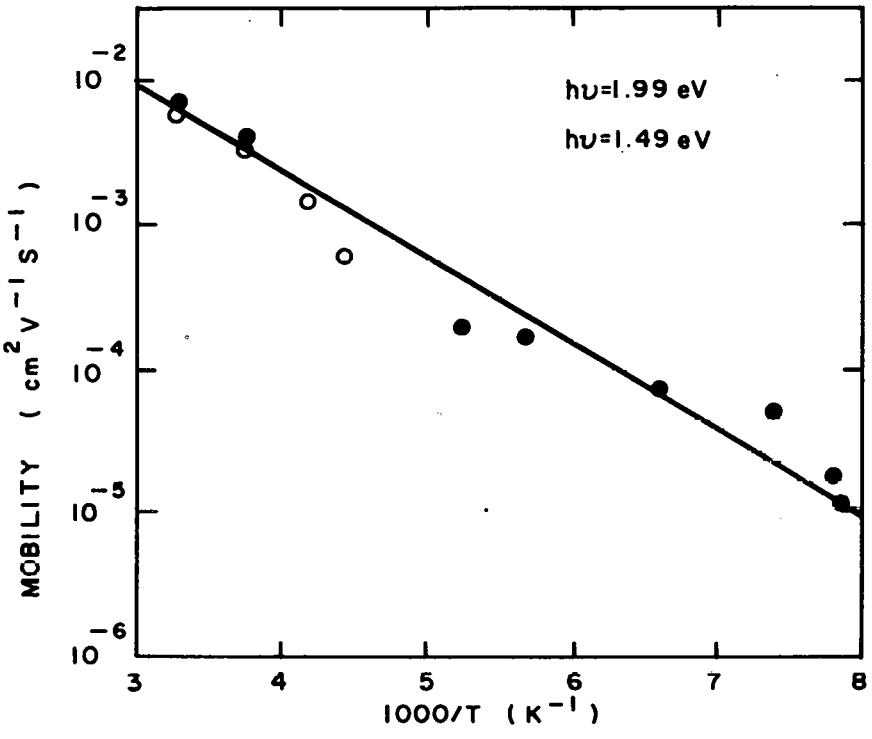

Figure 2-8. TEMPERATURE DEPENDENCE OF THE DRIFT MOBILITY MEASURED AT PHOTON ENERGIES ABOVE AND BELOW THE OPTICAL GAP

agreement with that found for μ_D by others [20-22]. The drift mobility has the same magnitude and temperature dependence for excitation above and below the bandgap.

Another observation from Table 2-1 is that τ_R increases by nearly a factor of 50 when the excitation energy is reduced from 1.49 to 0.99 eV. Since μ_D is the same at both excitation energies, the $\mu\tau$ product also increases by a factor of 50 over this range. This result is consistent with the data in Fig. 2-3.

2.5 DISCUSSION

Apart from the interference effects, the data in Figs. 2-3 and 2-4 can be represented by an Urbach tail to the optical absorption. This exponential dependence of the absorption coefficient on photon energy is widely observed

21. P. G. LeComber and W. E. Spear, Phys. Rev. Lett. 25, 509 (1970).
22. A. R. Moore, Appl. Phys. Lett. 31, 695 (1977).

in crystalline as well as amorphous material [23]. One explanation is that it is caused by random electric fields broadening the normally sharp absorption edge [23]. A similar explanation may apply here. Even though the absorption strength varies among the samples shown in Figs. 2-3 and 2-4, they exhibit the Urbach tail. This is shown by the broken lines drawn through the data points in curves a and b in Fig. 2-4. However, a property of the Urbach tail is that it has a characteristic temperature dependence of the form

$$\alpha = c \exp(\gamma h\upsilon/kT) \tag{2-6}$$

where γ and c are constants. Even though the absorption coefficient of a-Si:H shows the exponential dependence on $h\upsilon$ given by Eq. (2-6), it does not show the required temperature dependence. The various models [23] of the Urbach tail predict that the coefficient γ is the order of unity so that the activation energy for α would be over an order of magnitude larger than measured here.

An alternate interpretation for the observed optical absorption is that it represents transitions between the bandtail states. Field effect and other means have been used to measure the density of bandtail states [24,25]. Roughly, the data can be represented by a density of states N(E) decreasing exponentially away from the band edges. Its form is

$$N(E_1) = A \exp[(E_1 - E_c)/E_c^o] \tag{2-7}$$

where E_1 is the energy of the state below the conduction band edge (E_c), A is a constant, and E_c^o is the characteristic energy of the distribution. A similar expression applies near the valence band. The absorption coefficient will be proportional to the product of these densities of states and the matrix element (B) for the optical transition which is, in general, energy-dependent. Thus, as a function of E_1

$$\alpha(E_1) = B \exp\left[-(E_c - E_1 [1 - E_c^o/E_v^o])/E_c^o\right] \exp\left(\frac{h\upsilon}{E_v^o}\right) \tag{2-8}$$

23. N. F. Mott, and E. A. Davis, Electronic Processes in Non-Crystalline Materials (Clarendon Press, Oxford, England, 1971) p. 238.
24. W. E. Spear and P. G. LeComber, Philos. Mag. 33, 935 (1976); G. H. Dohler and M. Hirose, in Amorphous and Liquid Semiconductors, edited by W. E. Spear, (G. G. Stevenson Ltd., Dundee, Scotland, 1977) p. 372.
25. B. van Roedern, L. Ley, M. Cardona, and F. W. Smith, Philos. Mag. 13 40, 433 (1979).

where E_v^o is the characteristic energy of the valence band density of states. The absorption coefficient is obtained by integrating this equation over all E_1 consistent with energy conservation; i.e., $h\upsilon < E_1 < E_c$. The zero of energy is taken as the valence band edge. If we make the weak assumption that B varies slowly with E_1 compared with the exponential function of E_1 in Eq. (2-8) and replace it by its average value, then the absorption coefficient is

$$\alpha = C \exp (h\upsilon/E_v^o) \tag{2-9}$$

for bandtail absorption. Here, C is independent of $h\upsilon$. The absorption coefficient has this particular form because $E_v^o/E_c^o > 1$. Equation (2-9) shows that the important transitions are from states above the valence band to E_c. This is supported by the result that the majority carrier drift mobility determined from transient SPC measurements is independent of excitation energy. This argument does not depend on the detailed shape of the density of states but only that the density of states decreases more rapidly below the conduction band edge than above the valence band edge. The characteristic energies 0.1 and 0.09 eV for curves a and b in Fig. 2-4, respectively, are larger than the measured values for the conduction band [24], thus supporting our assumption that $E_v^o > E_c^o$. These values are also good representations of the field-effect density of states above the valence band [24,25].

The above result, which depends on the matrix element for the optical transition changing slowly with energy, shows that the optical absorption coefficient maps out the density of states above the valence band edge. Thus, optical absorption or primary photocurrent measurements can be a useful tool for studying gap states above the valence band. The three curves in Fig. 2-4 show that as phosphorus is added to a-Si:H, there is an increase in the states above the valence band. This is a surprising result because phosphorus is an n-type dopant. However, these results are consistent with those obtained by photoemission [25].

The above argument that the holes are produced far above the valence band, combined with the saturation with electric field of the primary photocurrent, shows that the holes are mobile even when deep in the bandtail states. An alternative would be to consider a two-step process in which the hole is excited to the valence band by a second photon. This process does not seem

likely to give as strong an optical absorption as observed. Also, one expects the photocurrent to then vary superlinearly with light intensity, whereas we observe a linear variation. That holes can conduct in bandtail states is not at all surprising. Hopping conduction near midgap has been observed in a-Si:H [26] with impurity densities on the order of those measured by field effect [24]. What is important for the primary photocurrent in a-Si:H is not the magnitude of the minority carrier mobility but the ratio of the recombination time to the transit time. If this ratio is much greater than unity, the primary photocurrent is maximized. Even though the mobility of the holes in these deep states will be low because of localization, the probability of these holes recombining with electrons is also low because of localization.

26. D. Allan, P. D. LeComber, and W. E. Spear, in Amorphous and Liquid Semiconductors, edited by W. E. Spear, (G. G. Stevenson Ltd., Dundee, Scotland 1977) p. 323.

SECTION 3.0

DEPOSITION AND DOPING STUDIES

3.1 dc PROXIMITY DEPOSITION SYSTEM

3.1.1 Effect of Substrate Temperature

In a recent report [2], we showed that the conductivity of phosphorus-doped films generally increased with increasing substrate temperature (T_s) up to the maximum temperature (~350°C) that was investigated. Figure 3-1 shows that the conductivity of boron-doped films also tends to increase with T_s, except for the most lightly doped case. We believe that the decrease in conductivity for T_s > 250°C (for $\beta = B_2H_6/SiH_4 = 1.3 \times 10^{-3}$) is caused by an increasing density of donor-like states as T_s increases. Undoped films become increasingly more conductive (and n-type) as T_s increases [27].

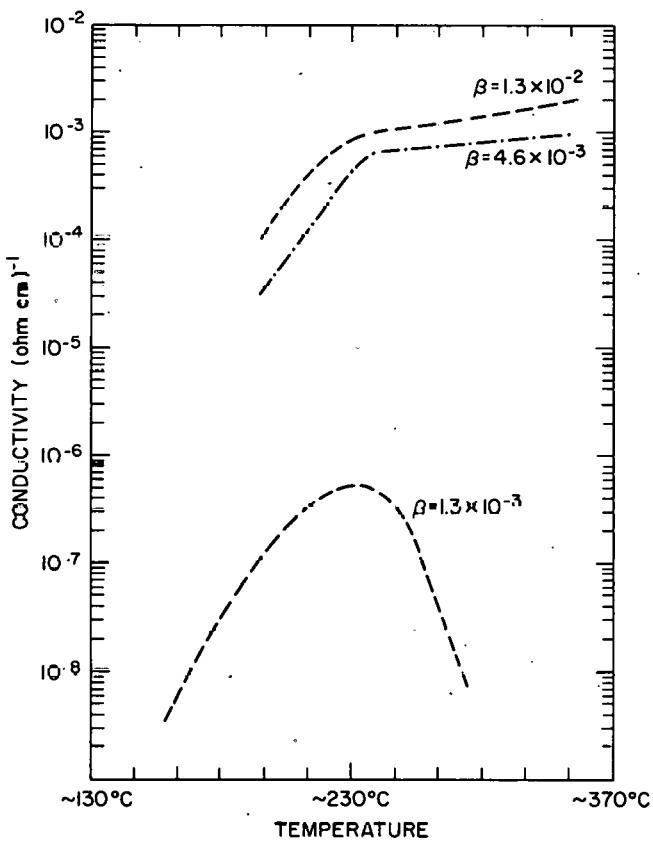

Figure 3-1. CONDUCTIVITY OF BORON-DOPED a-Si:H FILMS AS A FUNCTION OF SUBSTRATE TEMPERATURE FOR FILMS MADE IN A dc PROXIMITY DISCHARGE; $\beta = B_2H_6/SiH_4$

27. R. C. Chittick, J. Non-Cryst. Solids 3, 255(1970).

The photoconductivity of boron-doped films is small ($\sigma_p \tilde{\sim} 5 \times 10^{-7}\ \Omega^{-1}cm^{-1}$ at ~AM2 illumination for $\beta = 5 \times 10^{-4}$) and does not vary strongly with T_s over the range of 160° to 320°C. The photoconductivity of phosphorus-doped films is relatively large and tends to increase with T_s as shown in Fig. 3-2 for films made in an ac (60 Hz) proximity discharge; similar data was obtained in a dc proximity discharge.

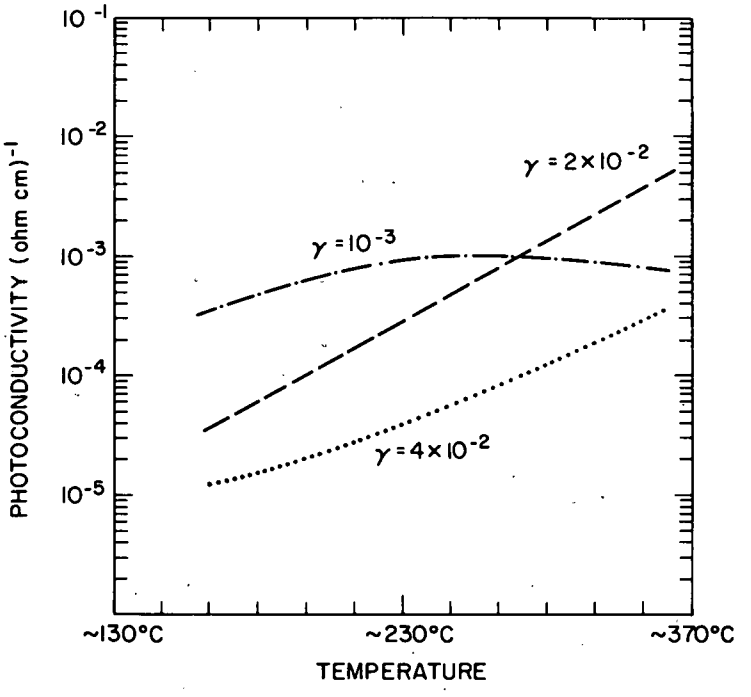

Figure 3-2. PHOTOCONDUCTIVITY OF PHOSPHORUS-DOPED a-Si:H FILMS AS A FUNCTION OF SUBSTRATE TEMPERATURE FOR FILMS MADE IN AN ac (60 Hz) PROXIMITY DISCHARGE, $\gamma = PH_3/SiH_4$

3.1.2 Effect of Discharge Power

In Fig. 3-3, we show a SIMS compositional profile of a layered sample where the discharge power was increased in steps from ~0.09 W/cm^2 to 0.70 W/cm^2; the top layer at a depth of 0 to 0.24 μm was deposited at the highest power. The substrate temperature was ~250°C and the discharge atmosphere was ~1.35% B_2H_6 in SiH_4. The data show an increase in contaminants (oxygen, nitrogen, and carbon) as the power is increased, probably as a result of sputtering at the SiO_2 discharge chamber walls. The boron concentration decreases from ~7 at.% to ~3.5 at.% as the discharge power increases. The hydrogen concentration increases

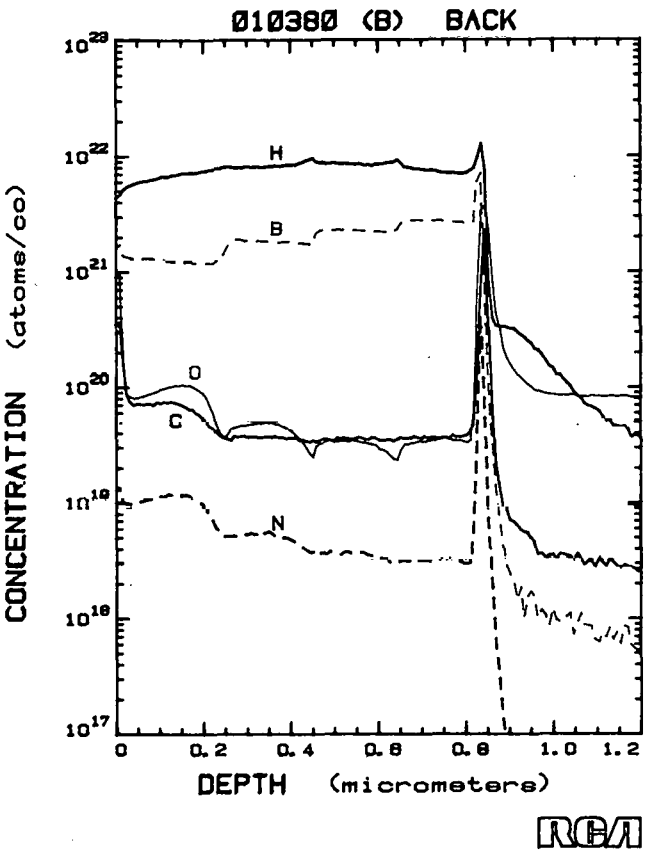

Figure 3-3. COMPOSITIONAL PROFILE OF A LAYERED SAMPLE WHERE THE DISCHARGE POWER WAS VARIED IN FOUR STEPS FROM 0.09 W/cm^2 TO 0.70 W/cm^2 (TOP LAYER)

at first (from ∿19 to ∿21 at.%) and then decreases (to ∿15 at.%) as the power increases.

In a similar experiment with 2% PH_3 in SiH_4, the phosphorus content decreased from ∿5.7 to ∿4.25 at.% as the power increased. In this case the hydrogen content increased slightly with power from ∿26 to ∿30 at.%.

The most conductive boron- and phosphorus-doped films were obtained for the low power conditions where the dopant concentrations were largest; σ was generally 2 to 5X larger for low power conditions over the range of $T_s \simeq 200°$ to 330°C than for high power conditions. Also, the reduction in hydrogen content observed at the lowest powers may reduce the concentration of dopant-hydrogen complexes (such as =B-H) since these centers may reduce the doping efficiency by creating gap states.

3.2 MASS SPECTROSCOPY OF THE rf DISCHARGE

3.2.1 Silane Discharge

We have continued studies of the positive ion composition of rf discharges using the line-of-sight mass spectrometer described previously [2]. We have done studies using both the magnetron mode and the asymmetric diode mode (the permanent magnet array removed from the cathode plate). The SiH_3^+ ion (m/e = 31) is usually the dominant one present, but significant quantities of higher Si content clusters ($Si_xH_y^+$ for x = 1 to 9) have been observed. These secondary ions are produced by reaction of the primary SiH_y^+ ions (y = 0 to 4) with the neutral SiH_4 molecules. Since we are dealing with a weakly ionized plasma, most of the silane in the discharge is neutral and provides a concentrated source of reactant.

The relative concentrations of the $Si_xH_y^+$ clusters have been studied as a function of pressure and rf power using both the magnetron and diode modes. The results are illustrated in Figs. 3-4 through 3-7 which show the relative intensities of clusters for x = 1 to x = 6. For both rf modes, the higher molecular weight clusters are favored by low rf power and high pressure, but the changes are more pronounced for the magnetron mode. We have also grown a-Si:H films on crystalline Si under the same conditions used for the positive ion mass spectra studies and have measured the infrared spectra of the films, from which we obtained the distribution of Si-H vibrational modes in the solid. A correlation is found showing that the larger the size of the $Si_xH_y^+$ cluster, the smaller the ratio of dihydride to monohydride species in the solid. The correlation is very strong for the magnetron deposition and somewhat weaker for the diode deposition.

There is good evidence that minimizing the dihydride species in the solid gives improved solar-cell characteristics - other things being equal [2]. Since low rf power and high pressure favors larger ion cluster size in the plasma, we should prepare solar cells at low rf power and high pressure.

We suggest the following model for a-Si:H film growth from these and earlier results. A $Si_xH_y^+$ ion landing on the surface recombines, and bond rearrangement and hydrogen atom migration away from the recombination site occur in the hot film. However, there is a higher probability of a $Si\text{-}H_2$ or $Si\text{-}H_3$ local cluster forming in the film, the larger the [H]/[Si] ratio in the

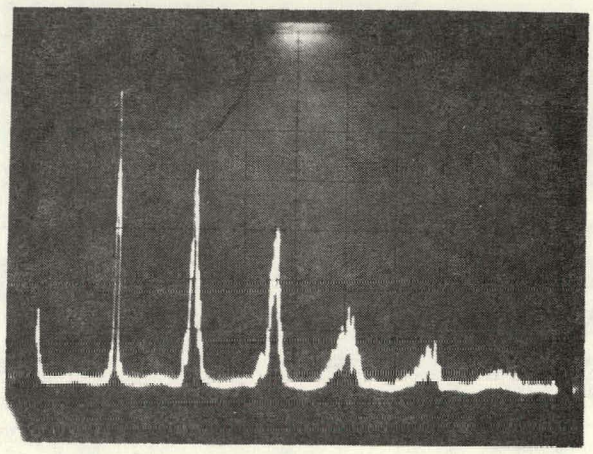

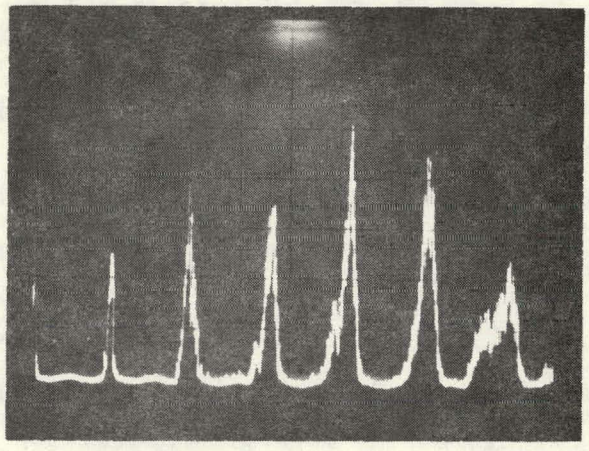

SILANE , MAGNETRON

Figure 3-4. ION INTENSITIES OF THE MASS CLUSTERS $Si_xH_y^+$ FOR x = 1 to 6, USING 75-W rf IN THE MAGNETRON MODE

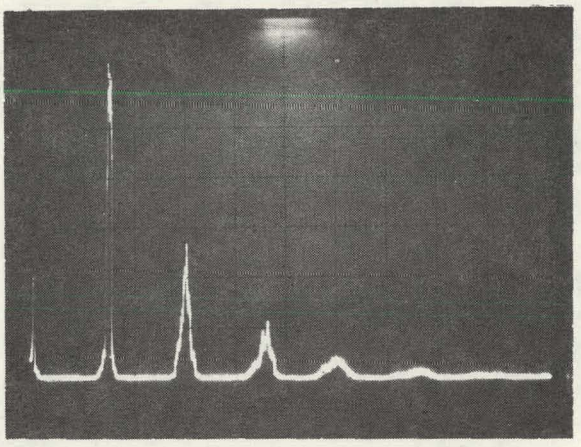

p = 6 mtorr 170 W rf

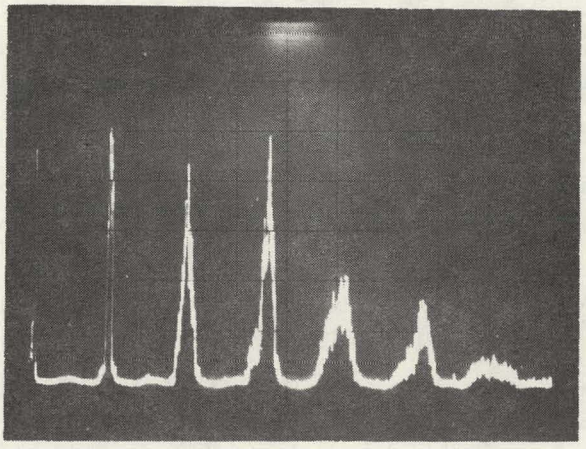

p = 10 mtorr 170 W rf

SILANE , MAGNETRON

Figure 3-5. ION INTENSITIES OF THE MASS CLUSTERS $Si_xH_y^+$ FOR x = 1 to 6, USING 170-W rf IN THE MAGNETRON MODE

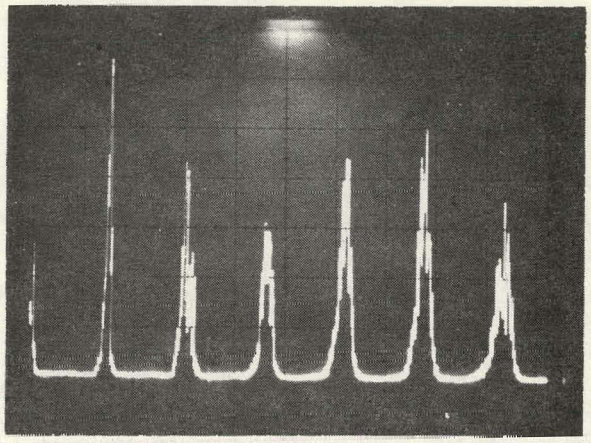

p = 16 mtorr 70 W rf

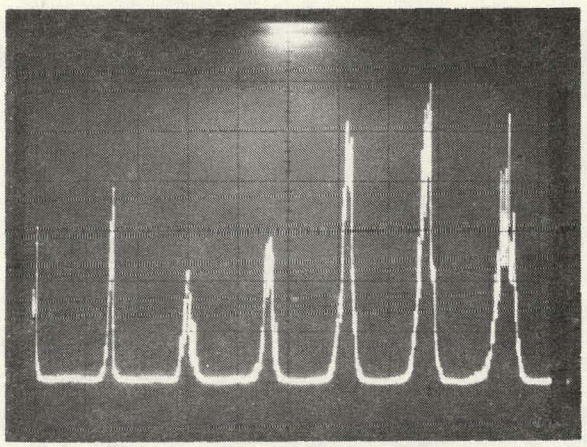

p = 30 mtorr 70 W rf

SILANE, DIODE

Figure 3-6. ION INTENSITIES OF THE MASS CLUSTERS $Si_xH_y^+$ FOR x = 1 to 6, USING 70-W rf IN THE DIODE MODE

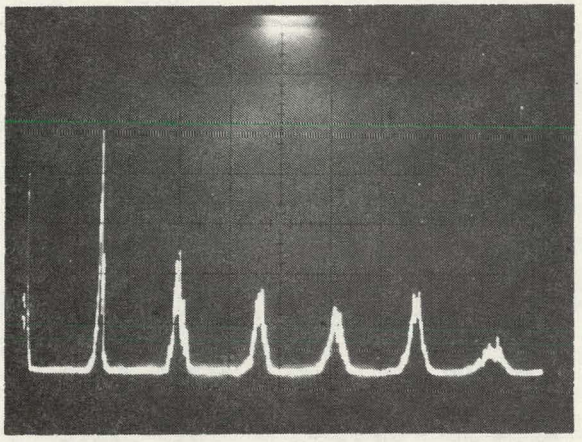

p = 14 mtorr 200 W rf

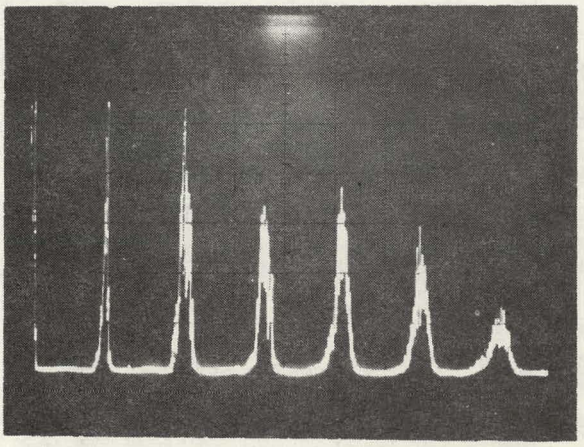

p = 35 mtorr 200 W rf

SILANE , DIODE

Figure 3-7. ION INTENSITIES OF THE MASS CLUSTERS $Si_xH_y^+$ FOR x = 1 to 6, USING 200-W rf IN THE DIODE MODE

molecular ion cluster. Earlier mass spectroscopic studies showed that the average ratio of [H] to [Si] decreases as the cluster size increases, tending toward a limit of [H] / [Si] = 2. Above a certain pressure, whose value may depend on the type of discharge, sufficiently large-sized clusters form and yield a polymeric powder which precipitates from the plasma.

We have also found that the concentration ratio $[SiH_2^+]/[SiH_3^+]$ is always less than unity for both modes under all the discharge conditions we have studied. The ratio is greater for the diode mode than for the magnetron mode and a typical comparison is shown in Fig. 3-8. The intensity scale of the vertical axis is linear and in order to show the less intense ion mass peaks for the magenetron mode, the main mass peak SiH_3^+ (m/e = 31) is off-scale. However, the concentration of SiH_2^+ (m/e = 30) may be estimated from Fig. 3-8 by comparison with the intensities of the peaks at m/e = 32 and 33. The latter two peaks consist almost entirely of the isotopes $Si^{29}H_3^+$ and $Si^{30}H_3^+$ and the naturally occurring abundance of silicon isotopes is Si^{28} = 92.2%, Si^{29} = 4.7%, and Si^{30} = 3.1%; hence, the concentration of SiH_2^+ is approximately 3%. We have found that the relative concentration of SiH_2^+ in the magnetron discharge depends sensitively on the bias potential of a substrate plate placed in front of the mass spectrometer sampling aperture (the substrate plate contains a hole to allow sampling of the discharge ions). This work is still in progress, but we have found that the $[SiH_2^+]/[SiH_3^+]$ ratio can be as large as 0.3 for the magnetron mode under certain conditions.

We also find that the $[SiH_2^+]/[SiH_3^+]$ ratio is large (greater than 0.5) for all conditions studied that use the diode mode and therefore, if the correlation between ion distribution in the plasma and film properties grown on substrates holds as suggested by the simple model described above, we should expect improved solar-cell performance for solar cells prepared using the rf diode mode. These studies have just begun.

3.2.2 Diborane-Silane Discharge

The positive ion spectrum of a discharge in a gas mixture 1% B_2H_6 + 99% SiH_4 shows that the concentration of ions containing boron are almost as great as that of the ions containing silicon. The concentration of $B_2H_5^+$ is approximately equal to that of SiH_3^+, and the ion $SiBH_4^+$ is itself approximately 1% that of the main silane ion, SiH_3^+. This preferential ionization of, or reaction of, boron with silane ions appears to be responsible for the observation

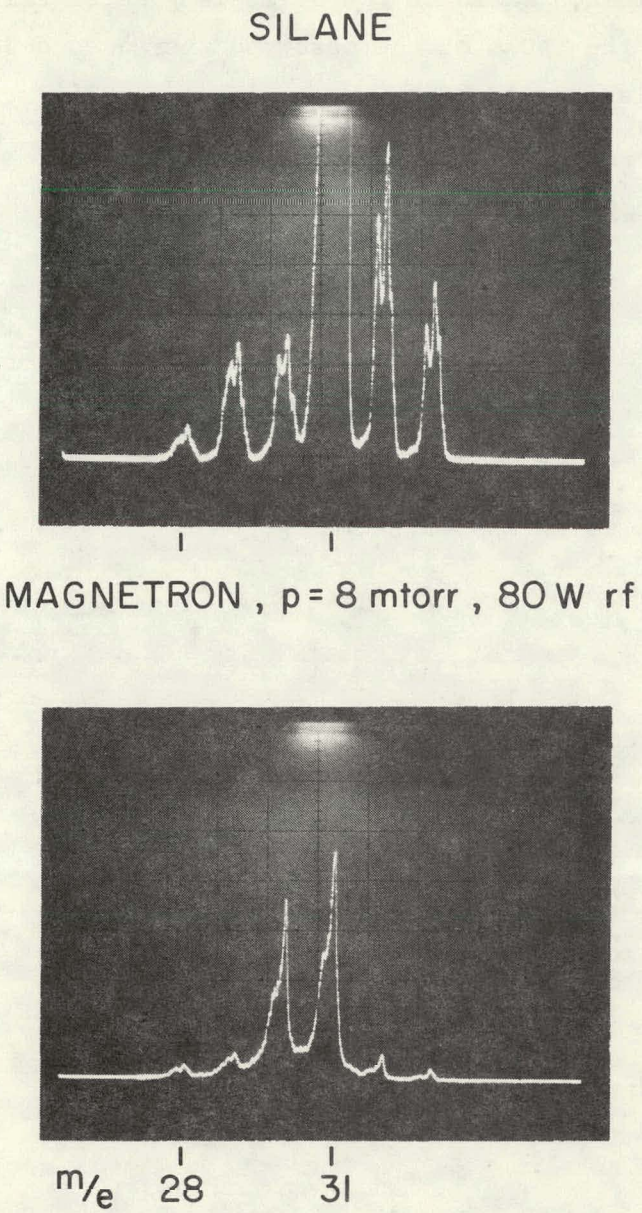

Figure 3-8. ION INTENSITIES OF SiH_y^+ FOR y = 1 TO 3 FOR THE MAGNETRON MODE AND THE DIODE MODE AT 80-W rf POWER

that the boron/silicon ratio in the films is greater than in the gas mixture, and must also be the cause of the observed increased deposition rate of films from diborane/silane discharges.

SECTION 4.0

EXPERIMENTAL METHODS FOR CHARACTERIZING a-Si:H

4.1 PHOTOLUMINESCENCE OF a-Si:H

The temperature dependence of the photoluminescence efficiency of undoped layers of a-Si:H was replotted to test the functional dependence reported by W. Paul at the San Diego SERI Workshop (January, 1980).

As shown in Fig. 4-1, a better fit is obtained to the function exp $(-T/T_o)$ where T_o = 28 K, than to exp (E_o/kT) where an activation energy E_o = 0.116 eV had been found. Whereas, E_o could be explained as the activation energy for a competing nonradiative recombination process, the significance of T_o is more difficult to explain.

An exponential dependence on T (instead of 1/T) is very rarely found in physical phenomena. To the best of our knowledge, such a dependence was discovered only for the variation of the threshold current in injection lasers [28]. The behavior was explained [29] on the basis of an exponential rise in absorption losses when the absorption edge shifts to lower energies faster than the emission peak. In a-Si:H, however, the emission peak and the absorption edge seem to shift at the same rate as in crystalline silicon.

4.2 HALL EFFECT IN UNDOPED a-Si:H

The purpose of these measurements and the current ideas about electron transport in a-Si:H were discussed in the previous report. In brief, one hopes to identify the mode of conduction and distinguish between the two models advanced in the literature: The first is the two-band model of the Dundee group, predicting electron conduction in extended states above 250 K. The second model, less clearly defined, has been proposed by the group at Marburg: it proposes that the electron mobility (μ) is thermally activated in the range of 200 to 600 K, and does not bring in the idea of a mobility gap.

During the last quarter the experimental procedure has been much improved, thus permitting μ to be measured at various illumination levels in the temperature range 200 to 600 K, and in the dark for a large part of that range.

28. J. I. Pankove, Radiative Recombinations in Semiconductors (Dunod. Paris, France 1964) p. 201.
29. J. I. Pankove, IEEE J. Quantum Electron. QE4, 119 (1968).

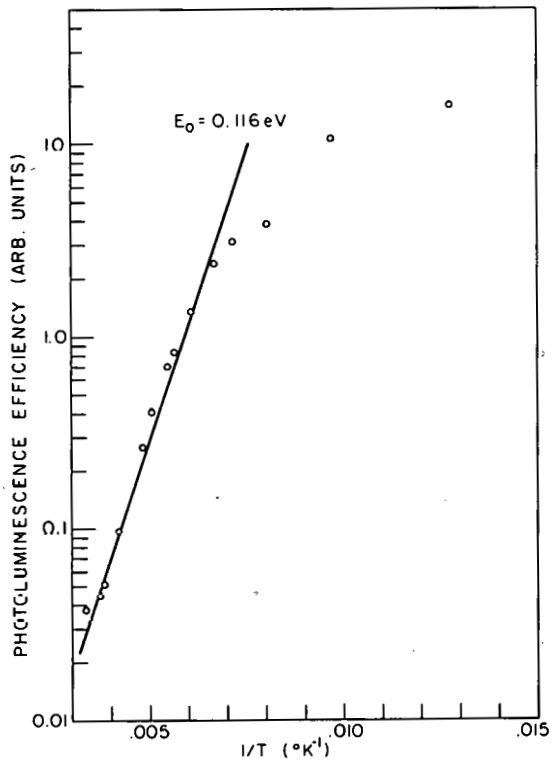

(a)

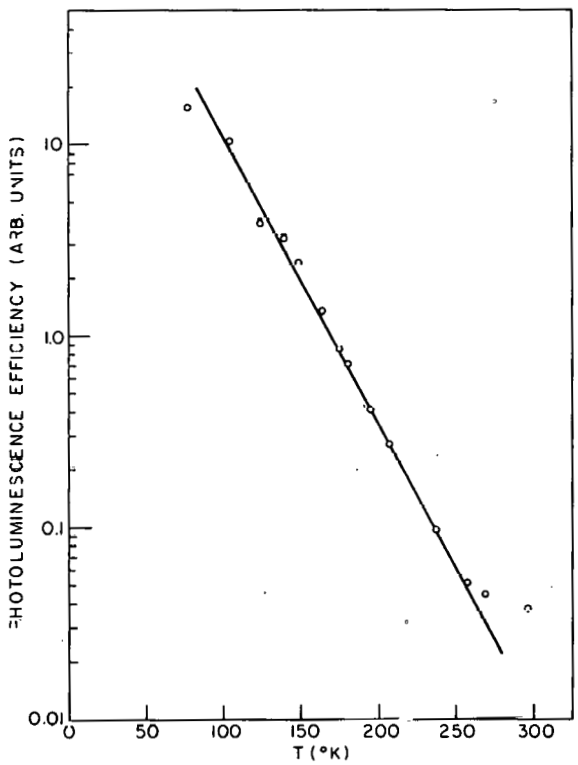

(b)

Figure 4-1. SEMILOGARITHMIC PLOTS OF THE PHOTOLUMINESCENCE EFFICIENCY AS A FUNCTION OF (a) 1/T, AND (b) T

Although analysis of the results presented below is far from complete, a new picture of electron conduction in a-Si:H is emerging.

These are the experimental results so far:

- The sign of μ_H is reversed (p-type) always. This agrees with measurements by others on doped a-Si:H samples.
- μ_H is independent of T below a transition temperature $T_t \tilde{\sim} 360$ K; above T_t, μ_H is thermally activated with energy E = 0.13 eV. At room temperature, μ_H is essentially independent of the light intensity from 0.07 mW/cm^2 to 40 mW/cm^2, where most measurements were performed. Furthermore, values of μ_H (dark) taken above T_t fall close to the curve at 40 mW/cm^2, although with a greater scatter of points.
- Examination of the photoconduction σ_1 vs T shows that below T_t the sample is in a light-soaked state and above T_t, is in the annealed state. This raises the possibility that the two mobility regimes might be connected with the Staebler-Wronski (S-W) effect. In this sample, the dark current, which has an activation energy of E$\sim$0.80 eV, is reduced only fourfold upon light-soaking. In this strongly compensated sample, the S-W effect manifests itself mostly on the photocurrent which drops tenfold upon light-soaking although $\gamma = 0.80$ is not changed. We have measured μ_H below T_t in the annealed state using a very low light intensity (0.14 mW/cm^2). The values of μ_H fell close to those in the light-soaked state ($\sim$0.1 cm^{2}V^{-1}s^{-1}). Hence, the two mobility regimes are not due to the S-W effect.
- Below T_t, the regime of constant μ_H, photoconductivity σ_1 is very weakly dependent on T(E = 0.03 eV). Thus, the carrier concentration remains nearly constant. Above T_t, a different conduction mode dominates where σ is thermally activated with E = 0.32 eV and μ with E = 0.13 eV.

Taken by itself, the behavior of μ and σ1 below T_t, as well as the reversed sign of μ_H, could be interpreted as transport in a disordered band of extended states, as proposed by the Dundee group. However, this model is now untenable since it is incompatible with an activated μ at higher temperature. The most reasonable conclusion from these measurements so far is that conduction below T_t takes place by tunneling in a band of states near the Fermi level. While

above T_t, the conductivity is dominated by thermally activated hopping. The fact that μ_H does not depend on light intensity in either regime suggests that only one band of states is involved in each regime; these two states are separated by 0.19 eV. However, their location relative to the band edges is, as yet, unknown.

4.3 PHOTOELECTROMAGNETIC EFFECT

When a photogenerated diffusion current of hole-electron pairs in a semiconductor interacts with an applied magnetic field perpendicular to the flow, an electric field appears at right angles to both the flow and the magnetic field. This is called the photoelectromagnetic (PEM) effect [30-32]. It is the Hall effect on an excess carrier diffusion current. The PEM effect was once widely used to characterize semiconductor materials for minority carrier lifetime and surface recombination velocity because it requires no p-n junctions, no applied electric fields, and no contacts in the path of the carrier flow. As grown single-crystal Ge and Si materials improved, the minority carrier lifetime in completed devices became limited by processes inherent in the device preparation itself, so the PEM method declined in favor of device-related approaches. The recent widespread interest in amorphous discharge-produced silicon (a-Si:H) for low-cost solar cells returns us to the era when the minority carrier properties are determined mainly by the semiconductor material preparation methods. Consequently, the PEM method may again be useful. We report here the first observation of the PEM effect in a-Si:H, estimates of mobility and lifetime obtained from it, and a discussion of the sign of the effect.

Hall and conductivity measurements on a-Si:H yield information about the majority carriers only (assumed here to be electrons). In photoconductivity (PC) also, the majority carrier predominates because of trapping of the minority carriers (holes), whence, the majority carrier $\mu\tau$ product is deduced. Yet

30. A review of both theory and experimental results, with references, can be found in Photo-Magneto-Electric Effect in Semiconductors by O. Garreta and J. Grosvalet, in "Progress in Semiconductors," Vol. 1 (Heywood and Co., 1956), p. 166.
31. A critical review of the theory is given by W. Van Roosbroeck, Phys. Rev. 101, 1713 (1956). The ambipolar concept is emphasized in W. Van Roosbroeck, Phys. Rev. 91, 282, (1953).
32. See also R. A. Smith, Semiconductor (Cambridge University Press, 1959) pp. 214-217.

in a solar cell, because of the barrier, the lifetime and diffusion length of the minority carrier is important in determining the collection efficiency, spectral response and conversion efficiency. The PEM effect in a photoconductor is basically a diffusion effect in which an internal field develops which forces free electrons and free holes to diffuse together (ambipolar diffusion) [31]. Even though most of the minority carriers may be trapped, the remaining untrapped holes control the diffusion. The pairs move with the diffusion coefficient and diffusion length of the minority carrier as in an extrinsic semiconductor. If all the holes were trapped, or if the free holes had a vanishingly small mobility, there could be no PEM effect. This ability to measure minority carrier motion even in the presence of a much larger photogenerated majority carrier concentration makes the PEM effect useful when the majority carrier lifetime is large compared to the minority lifetime, as in CdS [33], and InSb [34] at low temperature. However, most of the PEM literature is concerned with trap-free materials like crystalline Ge and Si in which the two lifetimes are equal and large and, therefore, easily observed.

The experimental configuration is shown in Fig. 4-2. Light from a mercury arc or a tungsten iodine lamp was focused onto the front face of the 5-mm-square, 2-μm-thick undoped a-Si:H sample mounted between the pole faces of a 4-in. electromagnet capable of providing a field up to 12000 gauss. Lines from the Hg arc and bands from the W-I lamp were isolated with filters. All measurements were made at room temperature. The high dark resistance of undoped material requires that the illumination spill over onto the contacts to prevent high resistance shadow areas. To avoid concomitant high photovoltages at zero magnetic field (offset voltage) good ohmic contacts are essential. The quartz substrate was first electroded with chromium, then a strongly n^+ phosphorus-doped a-Si:H layer was deposited by dc discharge on the electrode area only. Finally the undoped a-Si:H was deposited over the entire surface with a substrate temperature of 325°C. Offset voltages were from a half to a few times full scale, backed off by the zero control of the Keithley Electrometer. For short-circuit current the electrometer was used in the "fast"

33. H. S. Sommers, R. E. Berry, and I. Sochard, Phys. Rev. 101, 983 (1956).
34. R. N. Zitter, Phys. Rev. 112, 852 (1958) and R. N. Zitter, A. J. Strauss, and A. E. Attard, Phys. Rev. 115, 266 (1959).

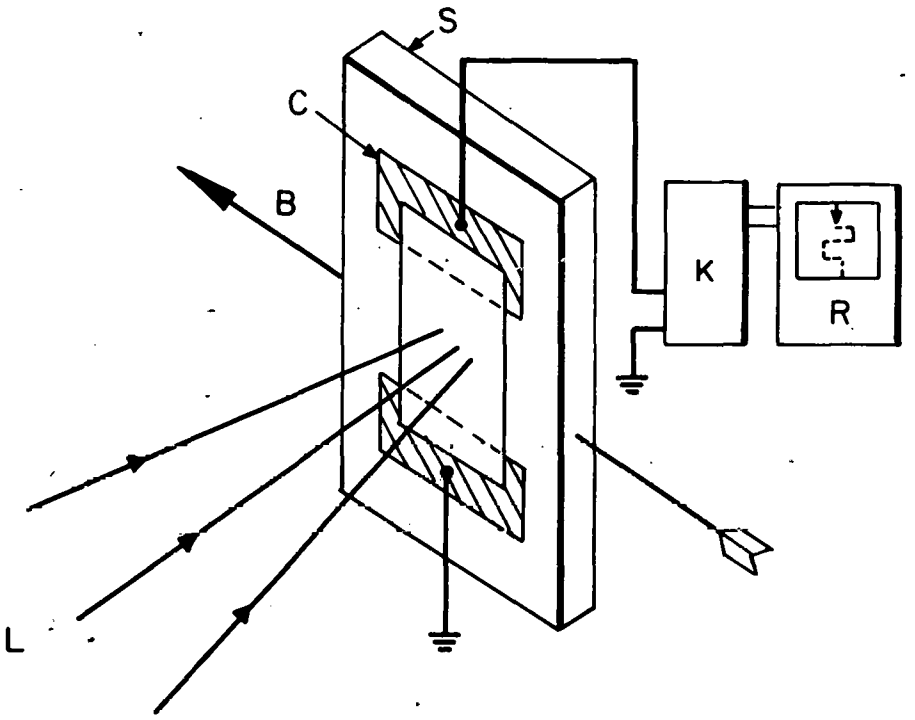

Figure 4-2. EXPERIMENTAL ARRANGEMENT, PEM EFFECT IN a-Si:H. SAMPLE IS ON QUARTZ SUBSTRATE S WITH CONTACTS C, IN MAGNETIC FIELD B. LIGHT BEAM L STRIKES FRONT FACE, SIGNAL READ BY KEITHLEY ELECTROMETER K AND RECORDER R

or feedback position, which lowers the effective input impedance of the meter to a value substantially less than the internal impedance of the illuminated sample. Open-circuit voltage was measured at 10^{14} Ω input resistance. Any residual offset voltage, its drift, and terms proportional to B^2, were canceled out by periodic reversal of the magnetic field and taking half of the signal difference. For an incident light intensity of about 10^{17} photons/cm^2-s at λ = 5770 Å and B = 10 KG, the short-circuit current was $\sim 10^{13}$ A.

Our belief that we are observing a true PEM short-circuit current is based on the following observations: (1) Reversal of the magnetic field reverses the sign of the current. (2) The component of the signal attributed to the PEM effect is proportional to the applied magnetic field. (3) The short-circuit current is approximately proportional to the light intensity over a range of nearly 100 to 1. (4) The observed current is largest for illumination with blue or green light, while red light is a very poor stimulus for the effect. This is to be expected in a true PEM effect, for when the reciprocal of the

optical absorption coefficient becomes larger than the diffusion length, the gradient of the pair concentration is reduced and with it the diffusion and the PEM current.

The quantitative expression of this last observation is shown in Fig. 4-3. We plot here the PEM gain (the external current per incident photon per second, corrected for reflection loss at the Si-air interface and at the quartz window) at 10-KG magnetic field as a function of energy and wavelength of the stimulating light. The corresponding photoconductive gain, similarly defined and measured at zero magnetic field with a 100-V battery in the external circuit, is also given. Both spectra cut off at the red end of the spectrum, but the PEM curve falls at higher photon energy. The fundamental reason for this is that the PEM current depends on a concentration gradient while the PC current is controlled by the total number of carriers (mainly majority) generated by the absorbed light, independent of their spatial distribution. The characteristic parameter defining the fall-off of concentration gradient is αL_p, where α is the optical absorption coefficient and L_p is the minority carrier diffusion length. Fall-off occurs when $\alpha L_p \leq 1$. On the other hand, the total number of majority carriers depends on $\alpha \ell$, where ℓ is the thickness. The PC current decreases when $\alpha \ell \leq 1$. Since it is known from solar-cell work that $\ell/L_p >> 1$, i.e., the diffusion length is short, αL_p becomes <1 where $\alpha \ell$ is still large. The result is that the PEM current falls more rapidly than the PC current as α is decreased by going to longer wavelengths. An even wider disparity has been observed in PEM experiments in crystalline Ge and Si, [30] and in InSb [32]. It was not observed [33] in CdS, however, because the absorption coefficient falls too rapidly in this direct bandgap material. a-Si:H represents an intermediate case.

There is also some fall-off in PEM current in the blue end of the spectrum. This was also occasionally seen in Ge, and being seen in CdS [35] was dismissed as unimportant. In any case, it is not predicted by standard PEM diffusion theory which assumes an idealization of uniform spatial lifetime and infinitely abrupt surface, conditions probably not met by real materials, especially a-Si:H. This complicates fitting the measurements to established formulas.

35. See footnote 6 in Ref. 4.

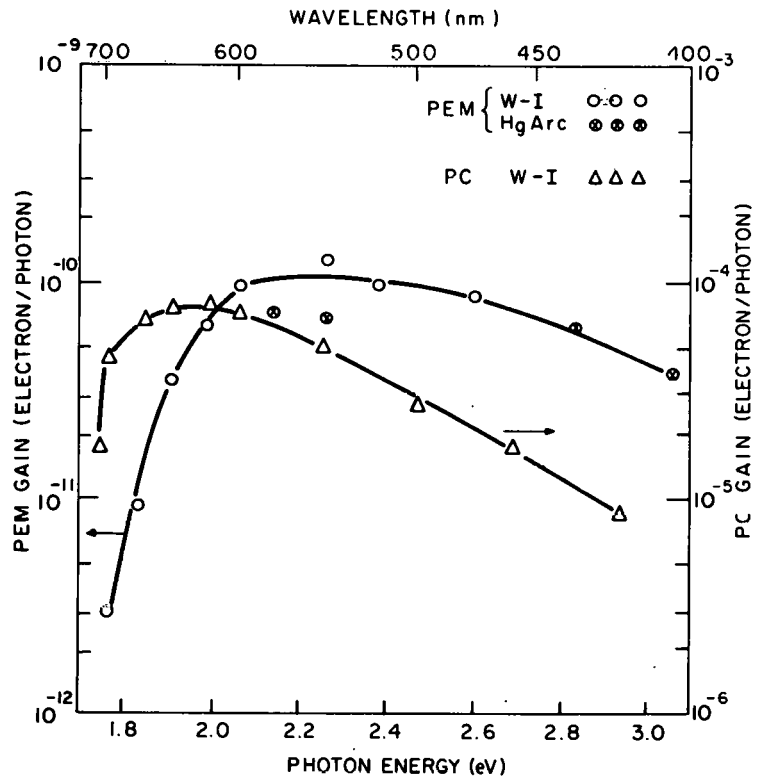

Figure 4-3. SPECTRAL RESPONSE OF THE PEM AND PC GAIN. PEM GAIN MEASURED AT 10 KG, PC GAIN AT 100 V APPLIED

The short wavelength difficulties are avoided if one measures the PEM open-circuit voltage. Since for a linear generator the open-circuit voltage is the short-circuit current divided by the conductance, we expect that the open-circuit voltage will saturate at high light levels where $\sigma_{photo} >> \sigma_{dark}$. This, too, was observed in crystalline materials [36]. That it is also seen in a-Si:H is demonstrated in Fig. 4-4 where V_{oc} is plotted vs relative light level for three different Hg arc wavelengths. Since both the PEM and PC currents fall off some in the blue, their ratio, which is the saturated value of V_{oc}, tends to remain constant in that region. In the red, as can be seen from Fig. 4-3, the ratio would decrease rapidly. Thus, the spectral distribution of saturated V_{oc} can be compared to the theoretically expected ratio $\alpha L_p/(1 + \alpha L_p)$. This comparison is shown in Fig. 4-5. The independently determined $\alpha(\lambda)$ has been folded into this curve. What is plotted for six different wavelengths is the saturated value of the PEM V_{oc} vs $\alpha\ell$. Also,

36. T. S. Moss, L. Pincherle, and A. M. Woodward, Proc. Phys. Soc., London, Sect. B 66, 743 (1953).

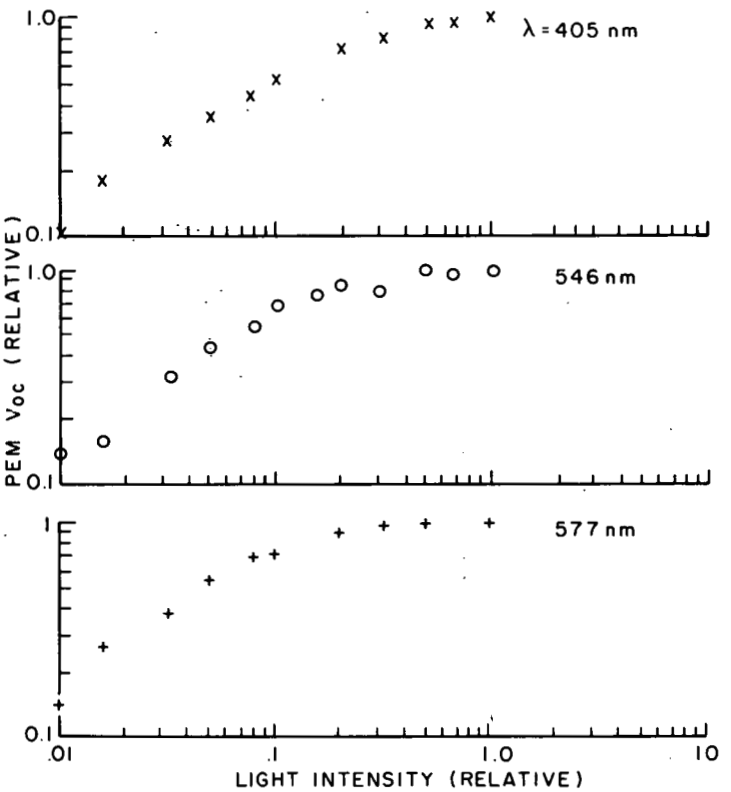

Figure 4-4. RELATIVE VALUES OF THE MEASURED PEM OPEN-CIRCUIT VOLTAGE vs RELATIVE LIGHT INTENSITY AT THREE DIFFERENT Hg ARC WAVELENGTHS

the function $\alpha L_p/(1 + \alpha L_p)$ is plotted vs αL_p. A best fit is obtained when $\alpha\ell/\alpha L_p = 23$, when, since ℓ is known, L is computed to be 0.09 μm. This measurement of the hole diffusion length has the advantage that it is independent of the absolute, or even the relative light level.

With the knowledge of L_p and the absolute light level, the remainder of the semiconductor parameters can be obtained from the PC and PEM I_{sc} and V_{oc}. For example, PEM theory gives $I_{sc} = 10^{-8}$ B w q μ_n (1 + 1/b)$I_o L_p$ assuming $\alpha\ell >> 1$ and small surface recombination. Here, I_o is the incident light intensity in photons/cm^2-s, w is sample width, and b is the ratio of electron to hole mobility. The latter constant was taken as equal to five from the Hall-effect measurements made in the dark on n- and p-type a-Si:H [37]. From

37. P. G. LeComber, D. I. Jones, and W. E. Spear, Philos. Mag. 35, 1173 (1977).

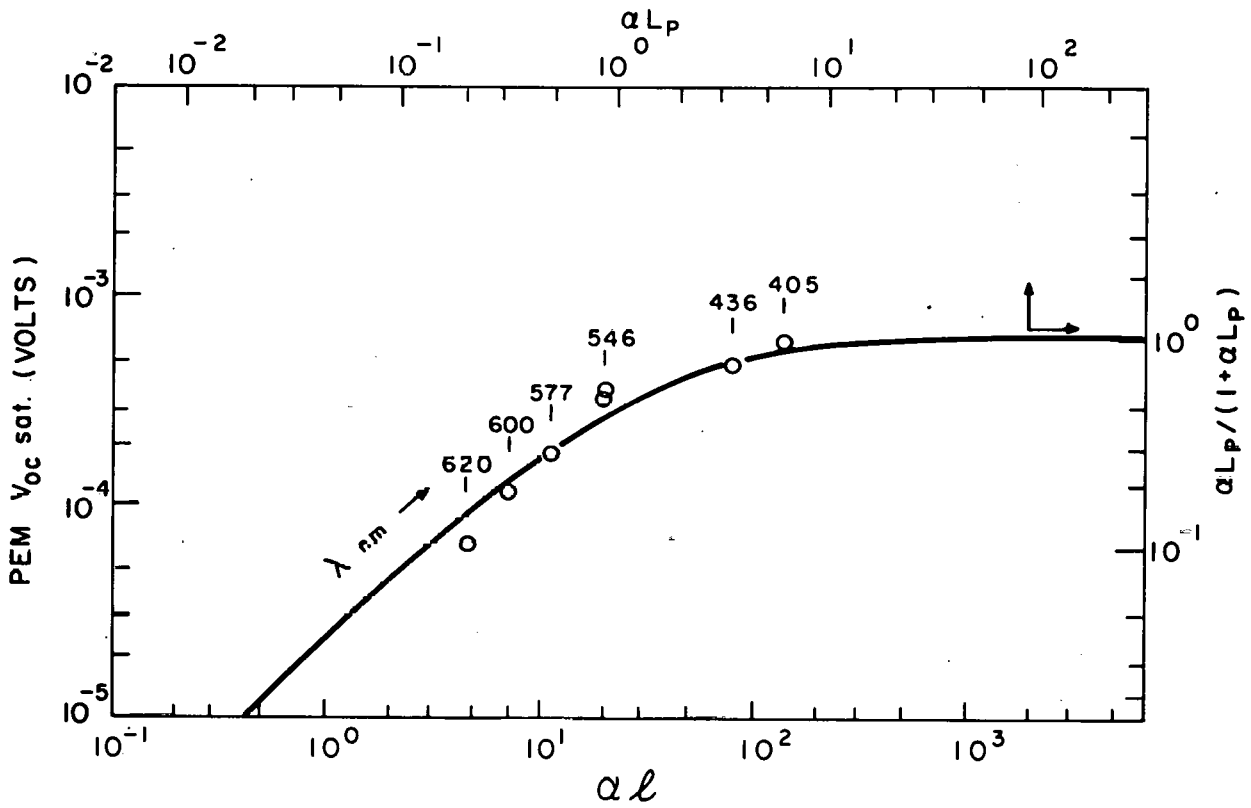

Figure 4-5. THE SATURATED VALUE OF THE PEM OPEN-CIRCUIT VOLTAGE AT 10 KG (LEFT SCALE) vs $\alpha\ell$ (LOWER SCALE, WITH $\ell = 2.06 \times 10^{-4}$ cm). THE SOLID LINE IS THE FUNCTION $\alpha L_p/(1+\alpha L_p)$ (RIGHT SCALE) vs αL_p (UPPER SCALE)

the observed I_{sc} at the maximum (Fig. 4-3) we find $\mu_n = 4.6 \times 10^{-2}$ cm^2/V-s, and with the value of b above, $\mu_p = 9.2 \times 10^{-3}$ cm^2/V-s. From the PC, $(\mu_n\tau_n) = 7.8 \times 10^{-8}$ cm^2/V at the 546-nm Hg line, whence $\tau_n = 1.7 \times 10^{-6}$ s. On the other hand, $\tau_p = L_p^2/D_p = L_p^2/(kT\mu_p/q) = 3.4 \times 10^{-7}$ s. An internal check on τ_n can be obtained from the measured saturated open-circuit voltage at the same wavelength. The result comes out $\tau_n = 1.2 \times 10^{-6}$ s, in satisfactory agreement. Thus, the ratio of majority to minority carrier lifetime is about five to one. From detailed balance, $n/p = \tau_n/\tau_p$, so one can state crudely that there is one free hole for each five free electrons, while four holes are trapped. Again a-Si:H appears to be intermediate between CdS-type insulating semiconductors and classical semiconductors like crystalline Si.

Since the pair diffusion current consists of equal and opposite electric currents of holes and electrons, the sign of the PEM effect should be the same for n- and p-type materials. When n- and p-type samples of crystalline Si

were used in our apparatus it was found, unexceptionally, that this was true. But more importantly, the sign was the same as obtained with a-Si:H samples. This seemingly normal result is unusual because of the report [37] that the sign of the Hall effect in the dark in both n- and p-type a-Si:H is reversed from normal. With inverted Hall coefficient for both electrons and holes, the PEM effect should also be inverted, contrary to observation. Based on diffusion theory, it is possible in principle to get a reversed PEM effect (that is, normal, if the Hall coefficients are inverted) if the diffusion current flows backward toward the illuminated surface, as could be the case if the surface recombination velocity at the front were greater than at the rear. To test for this possibility, the sample was turned around and illuminated through the substrate. The sign remained unchanged. Also, a simple surface etching trial showed no large effect.

Our result is consistent with Friedman's [38] original random-phase model in which he found that for diffusive transport in the extended states near the mobility edge, the Hall-effect sign would be normal for electrons but inverted for holes. As long as the magnitude of the hole mobility is appreciably less than that of electrons, the sign of the PEM effect will be dominated by electrons. The magnitude of μ_n also agrees. In a later paper [39], and one of Emin [40], the possibility of p-like orbitals in the electron hopping motion is shown to allow also a reversal of electron Hall coefficient, consistent with LeComber et al. [37]. But neither of these considers the possibility of photo-stimulated carriers which may move much higher up in the band than thermal equilibrium carriers (dark). Furthermore, in the PEM effect the holes and electrons move together in close physical proximity. The extent to which this may influence the local wave functions which constitute the extended state, particularly if the mean free path is of the order of a lattice spacing or greater, is not clear at present.

38. L. Friedman, J. Non-Cryst. Solids 6, 329 (1971).
39. L. Friedman, Philos. Mag. 38, 467 (1978).
40. D. Emin, Philos. Mag. 35, 1189 (1977).

SECTION 5.0

FORMATION OF SOLAR-CELL STRUCTURES

5.1 LARGE-AREA MONOLITHIC SOLAR-CELL PANEL

A 16-cell, series-connected, a-Si:H monolithic solar panel has been fabricated on a 4" x 4" glass substrate. The cell structure consisted of glass/ITO/Pt-SiO_2 cermet/p-i-n a-Si:H/Ti, and it was illuminated through the glass. For the deposition of the cermet and a-Si:H layers, optimized parameters reported previously have been used*. The solar panel was encapsulated in a plastic frame as shown in Fig. 5-1; the active area was 63 cm^2. The J-V curve and the performance data are shown in Fig. 5-2. The efficiency (η) of 3.6% is the highest reported to date for an a-Si:H panel or cell of this size.

5.2 OPTIMIZATION OF n- AND i-LAYER THICKNESSES FOR CELLS ILLUMINATED THROUGH THE n-LAYER

In Quarterly Report No. 1 (Ref. 41, pp. 39 and 40), we have shown that for a p-i-n cell illuminated through the n-layer as opposed to the p-layer, the short-circuit current density (J_{sc}) and η nearly doubled. This large increase in performance is most likely due to more light getting into the active region. This result prompted us to perform an optimization study of the a-Si:H n- and i-layer thicknesses, by means of thickness-graded cells used in this program. The cell structure consisted of glass/Cr (270 nm)/Pt-SiO_2 (10 nm)/p (8 nm)/i (315-879 nm)/n (0-68 nm)/Ti (3 nm)/ITO (75 nm). The i- and n-layers were graded normal to each other, and all a-Si:H layers were deposited in an rf capacitive discharge system. The ITO was E-beam evaporated; it had sheet resistivity of about 300 Ω/□. The doping level for the n-layer was 1.3% PH_3 in SiH_4; and for the p-layer, 0.6% B_2H_6 in SiH_4.

The performance data including V_{oc}, J_{sc}, fill factor (FF), η, and series resistance (R_4) at 1-V forward bias are shown in the form of contours as a function of n- and i-layer thicknesses in Figs. 5-3 through 5-7, respectively. When

*For the cermet, see p. 104 of Ref. 2, and for the a-Si:H, see p. 34 of Ref. 41.

41. D. E. Carlson, R. S. Crandall, J. Dresner, B. Goldstein, J. J. Hanak, A. R. Moore, J. I. Pankove, and H. A. Weakliem, Quarterly Report No. 1, SERI/PR-9-8254-1, prepared for the Solar Energy Research Institute under Subcontract No. XJ-9-8254.

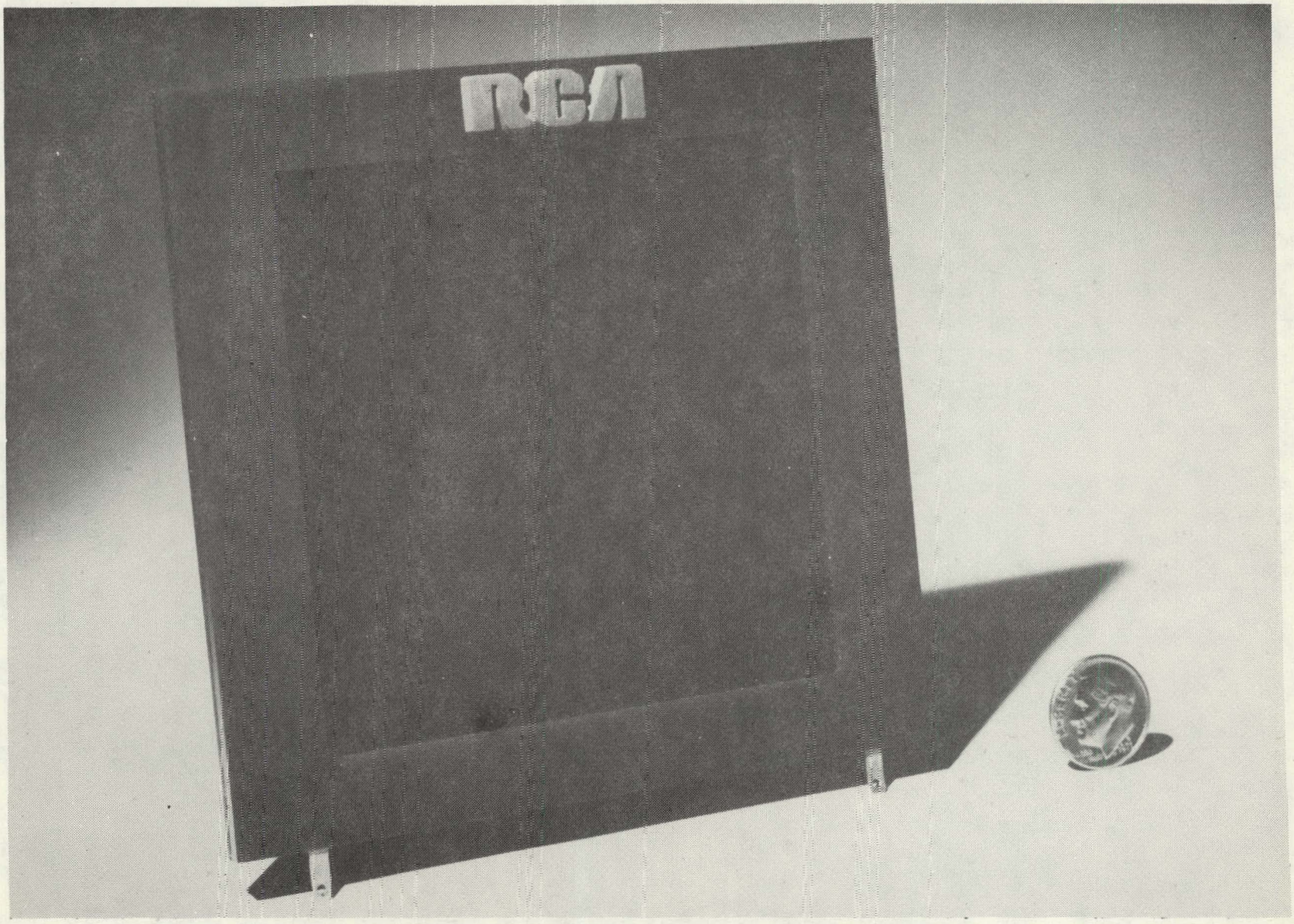

Figure 5-1. PHOTOGRAPH OF A MONOLITHIC AMORPHOUS SILICON SOLAR-CELL PANEL CONSISTING OF 16 CELLS IN SERIES FABRICATED ON A 4" X 4" GLASS SUBSTRATE (ACTIVE AREA = 63.2 cm^2)

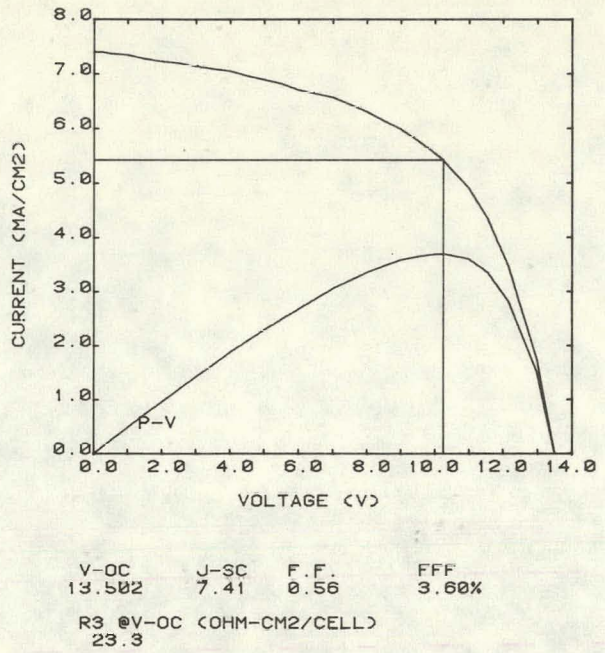

Figure 5-2. J-V CURVE AND PERFORMANCE DATA FOR THE MONOLITHIC SOLAR-CELL PANEL OF FIG. 5-1 UNDER 95% AM1 ILLUMINATION

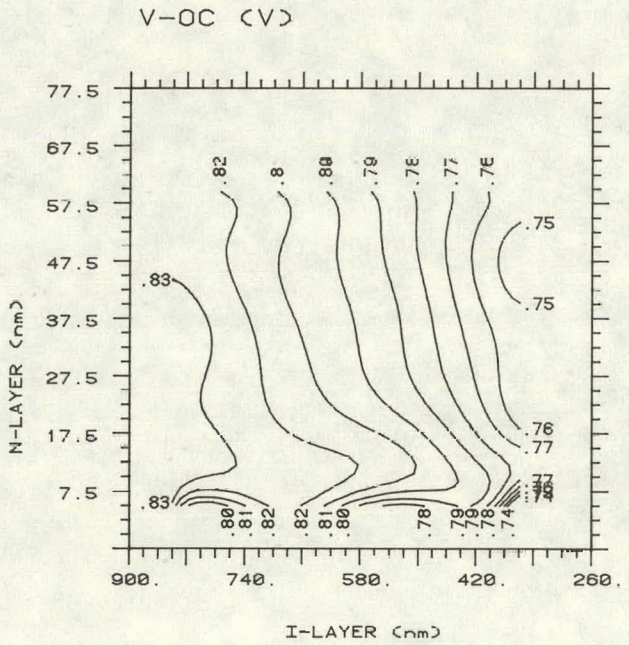

Figure 5-3. CONTOURS OF V_{oc} AS A FUNCTION OF THICKNESS OF THE a-Si:H n- and i-LAYERS OF A p-i-n CELL STRUCTURE ILLUMINATED THROUGH THE n-LAYER

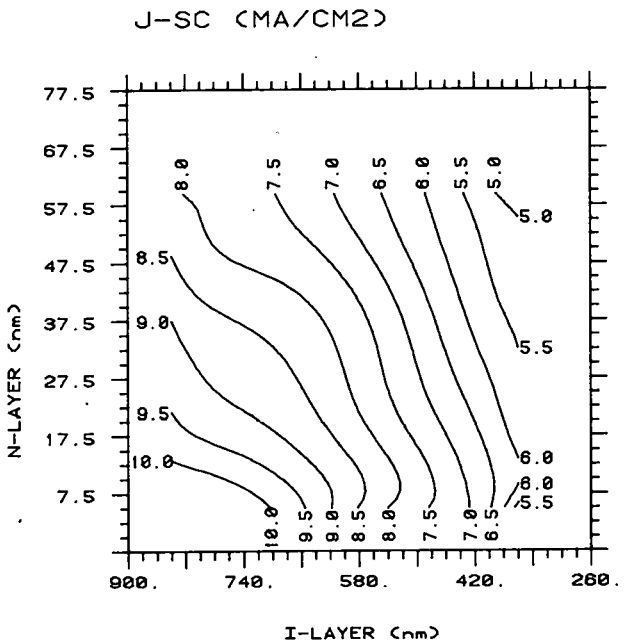

Figure 5-4. CONTOURS OF J_{sc} AS A FUNCTION OF THICKNESS OF THE a-Si:H n- AND i-LAYERS OF A p-i-n CELL STRUCTURE ILLUMINATED THROUGH THE n-LAYER

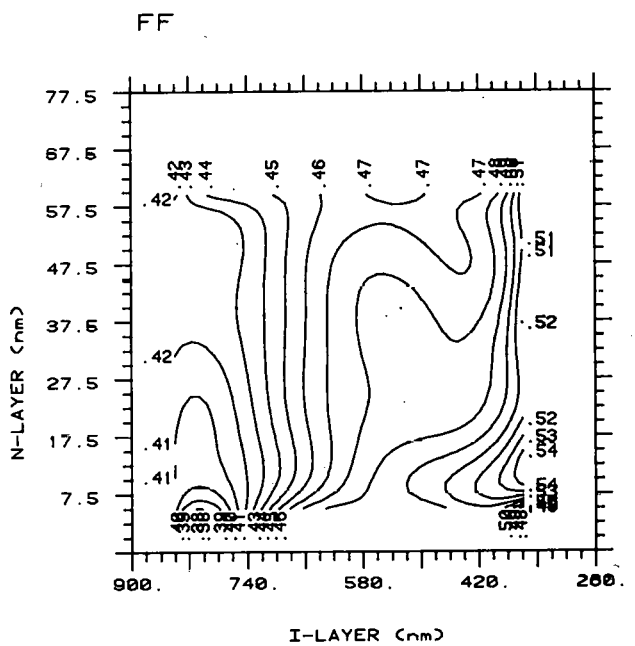

Figure 5-5. CONTOURS OF FF AS A FUNCTION OF THICKNESS OF THE a-Si:H n- AND i-LAYERS OF A p-i-n CELL STRUCTURE ILLUMINATED THROUGH THE n-LAYER

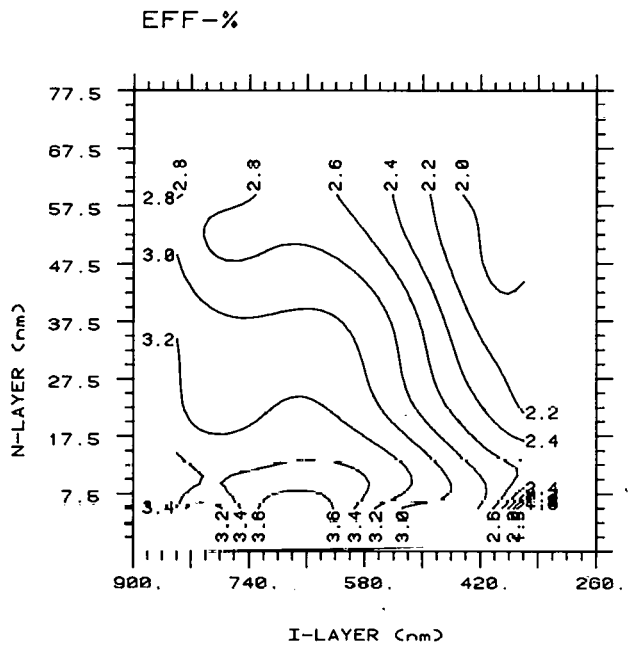

Figure 5-6. CONTOURS OF η AS A FUNCTION OF THICKNESS OF THE a-Si:H n- AND i-LAYERS OF A p-i-n CELL STRUCTURE ILLUMINATED THROUGH THE n-LAYER

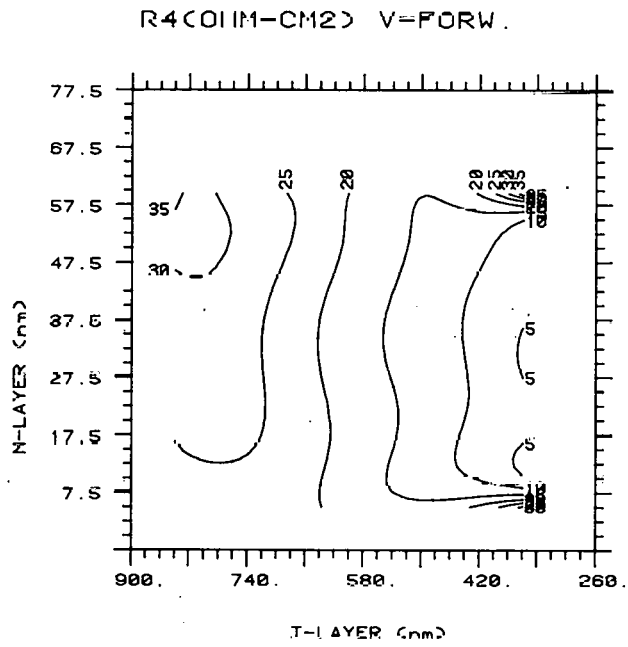

Figure 5-7. CONTOURS OF R_4 AS A FUNCTION OF THICKNESS OF THE a-Si:H n- AND i-LAYERS OF A p-i-n CELL STRUCTURE ILLUMINATED THROUGH THE n-LAYER

compared with the performance data for i-n cells illuminated through the n-layer (Ref. 41, pp. 31-38), several differences clearly stand out. In the present case, the V_{oc} increases perceptibly with the i-layer thickness, whereas in the previous case, it is constant. In the present case, R_4 increases and FF decreases significantly with increasing i-layer thickness, whereas, in the previous case, both show little dependence. This difference is due to the fact that in the present case, most of the holes are formed closer to the n-layer and, hence, must traverse much larger thicknesses of the i-layer than in the previous case. Because of the low diffusion length, progressively more holes become trapped with increasing i-layer thickness which results in rapidly increasing R_4 and consequently, decreasing FF. Thus, although both V_{oc} and J_{sc} increase with the i-layer thickness, the maximum in η occurs at intermediate thicknesses ($\sim$600 nm). As expected, J_{sc} and η show an inverse dependence on the n-layer thickness, for which the optimum is at $\lesssim$5 nm.

Significant increases in efficiency above the value of 3.6% (Fig. 5-6) are expected because both J_{sc} and FF can be increased, respectively, by eliminating the 3-nm-thick Ti layer and by increasing the conductivity of the ITO layer.

5.3 EQUIPMENT ENHANCEMENTS

A new rf sputtering- rf (capacitive) discharge deposition system has been installed at RCA Laboratories. The new system has three targets and is capable of depositing the entire solar-cell structure in one pumpdown. Up to 45 3" x 3" substrates can be mounted on a moving substrate holder and deposited in one run. Graded doping along the surface of the substrate during glow-discharge deposition is a new feature not present in our other deposition systems. The system is now being calibrated for deposition temperature profiles and deposition rates.

5.4 SOLAR-CELL PREPARATION USING THE rf MAGNETRON MODE

Solar-cell performance for the magnetron-produced cells is steadily improving with time; however, it must be noted that the best results are not as good as those of the best cells produced by others using the dc proximity, or rf diode

techniques. A summary of the results of several types of cells, is shown in Table 5-1 below:

TABLE 5-1. SOLAR-CELL CHARACTERISTICS

Date Prepared	Type	V_{oc} (V)	J_{sc}(mA/cm^2)	FF	Efficiency (%)
10/15/79	Pt/p/i/n/Mo	0.5	1.0	0.28	0.15
10/25/79	Pt/i/n/S.S.	0.40	4.5	0.45	0.8
12/5/79	ITO/i/n/S.S.	0.45	7.2	0.45	1.5
12/9/79	ITO/n/i/p/S.S.	0.72	6.0	0.42	1.8
1/15/80	ITO/n/i/p/S.S.	0.76	6.2	0.47	2.2
1/18/80	ITO/n/i/p/S.S.	0.77	6.2	0.52	2.5

(S.S. is stainless steel).

A number of improvements were made on the deposition system during this period, including a newly designed gas inlet system which introduces and distributes the gas near the region of the active glow discharge.

We have made the necessary connections to enable the use of the line-of-sight mass spectrometer as a sensitive He leak detector. We have calibrated the sensitivity to be $\sim 5 \times 10^{-10}$ atm-cc/s, which compares favorably with high-quality He leak detectors. We have found and sealed several small leaks in the gas manifold and one leak in a weld joint of the stainless steel chamber. This latter leak corresponded to a partial pressure of 3×10^{-8} Torr in the chamber, taking into account the known pumping speed of the system. SIMS analysis on a sample prepared after these leaks were sealed showed very low impurity concentrations (oxygen 400 ppm, and nitrogen 40 ppm).

a-Si:H deposition studies using the rf diode mode have been started. The initial work is concerned with the establishment of the range of possible operating parameters, pressure, rf power, and flow rate.

5.5 OPTIMIZATION OF p-i-n DEVICES MADE IN A dc(P) DISCHARGE

5.5.1 Structures

Figure 5-8 shows two variations of the inverted p-i-n structure that are currently being optimized. In both cases, the p-layer is deposited first, then the undoped layer and the n-layer. If the cell is illuminated through the n-layer, the top contact is electron-beam evaporated ITO (indium-tin-oxide)

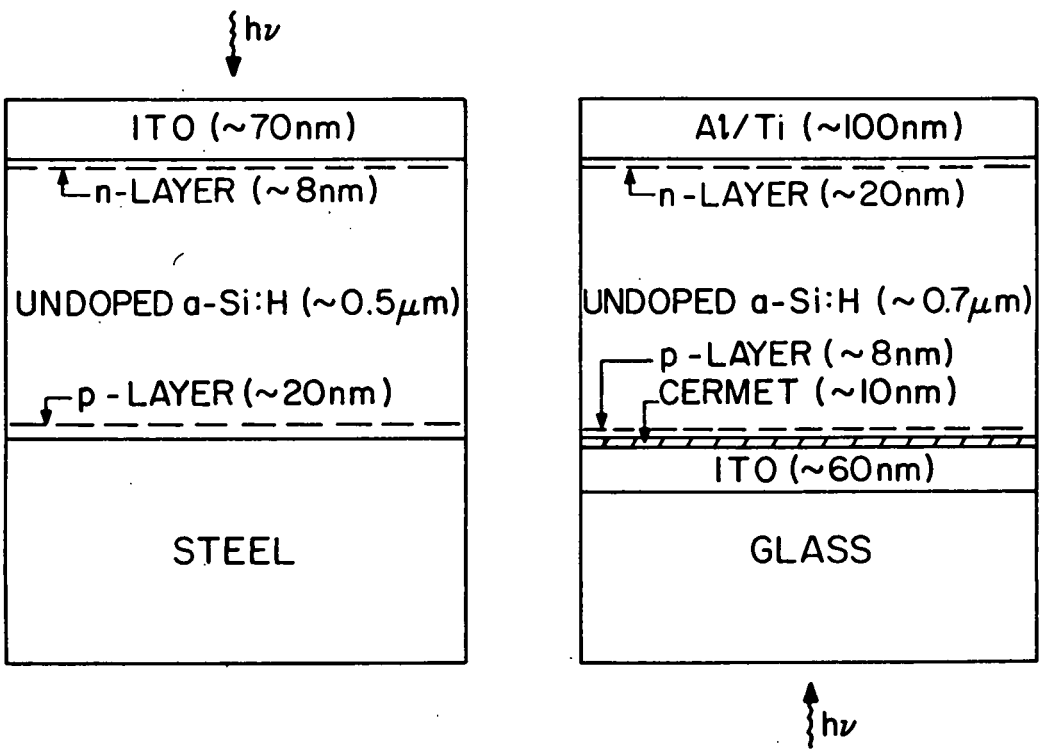

Figure 5-8. p-i-n STRUCTURES.

and the substrate may be stainless steel. However, if the cell is to be illuminated through the p-layer, the substrate is ITO-coated glass with a thin cermet contacting layer and the top contact is an opaque film of sputtered Ti or Al/Ti [2].

5.5.2 SIMS Profile

A compositional profile of an inverted p-i-n structure on steel is shown in Fig. 5-9. This profile was obtained by secondary ion mass spectroscopy (SIMS) where the concentrations were determined by means of ion implantation standards [42]. The cell exhibited a conversion efficiency of 3.49% (V_{oc} = 798 mV, J_{sc} = 8.4 mA/cm^2 and FF = 0.524); the area was 1.19 cm^2.

A small air leak was present in the SiH_4 line when the cell was fabricated. Thus, the oxygen and nitrogen concentrations are relatively low in p-layer

42. C. W. Magee, RCA Laboratories, Princeton, NJ.

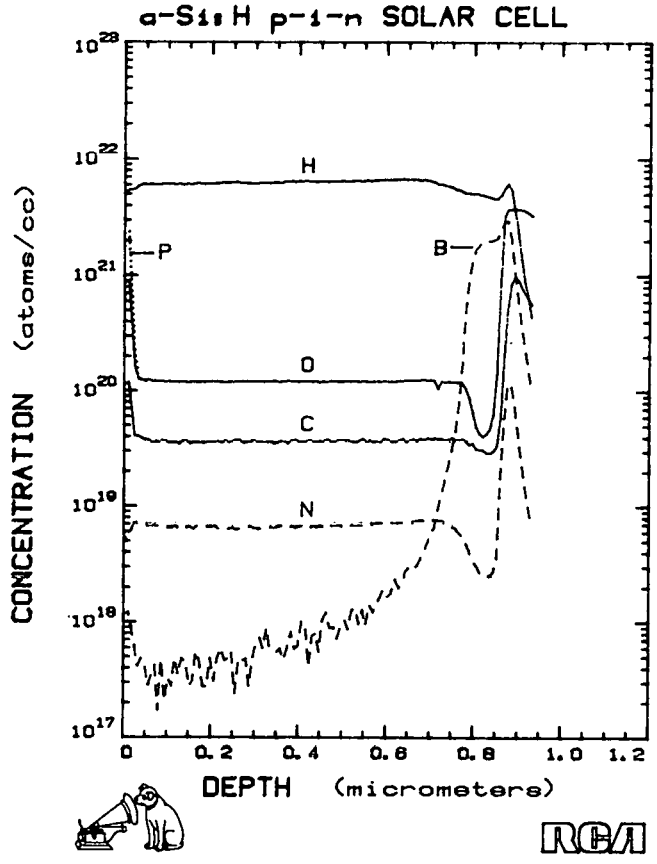

Figure 5-9. COMPOSITIONAL PROFILE OF A p-i-n CELL

(where 1.35 vol % B_2H_6 in SiH_4 was the source) and both increase as the "pure" SiH_4 flow is turned on. Other profiles have shown oxygen concentrations as low as $10^{19}cm^{-3}$, and nitrogen concentrations as low as $\sim 10^{18}cm^{-3}$.

The profile also shows ~10 ppm of residual boron in the bulk of the device. Another experiment showed that relatively small amounts of boron (~40 ppm) in the bulk of the device caused the efficiency to drop by ~40% (J_{sc} fell by ~20% and V_{oc} by ~13%). Earlier work had shown that small amounts of phosphorus (~20 ppm) in the bulk could cause a significant reduction in the performance [1].

5.5.3 Effect of Substrate Temperature

A series of p-i-n devices were made at substrate temperatures (T_s) varying from 250° to 390°C. Five p-i-n devices (each 1.19 cm^2) were made on each steel substrate (3" x 3"), and the efficiency of the best device is plotted in Fig. 5-10 as a function of substrate temperature. The data clearly show that

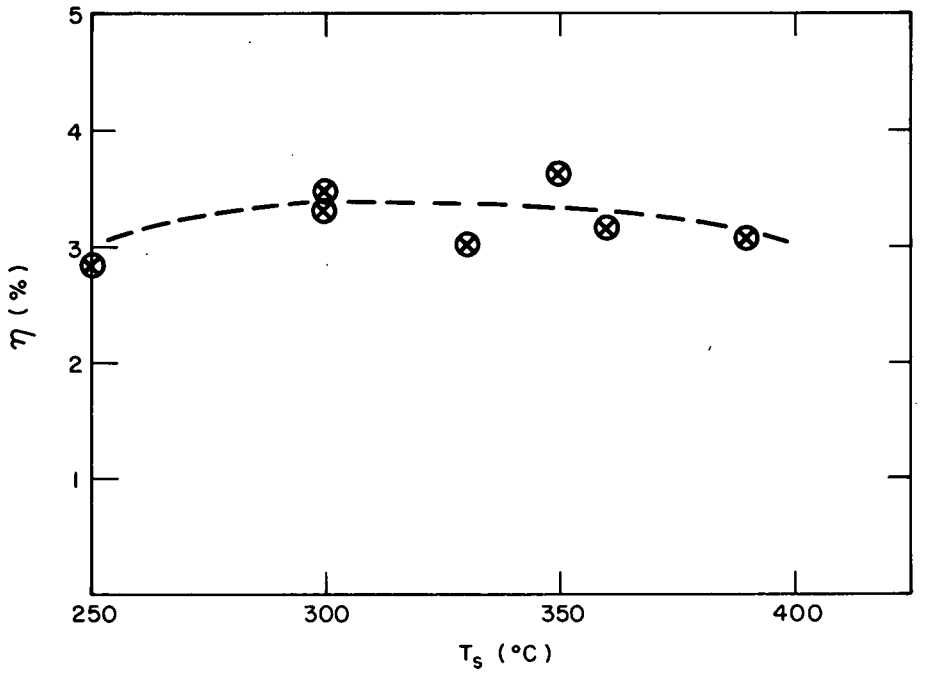

Figure 5-10. CONVERSION EFFICIENCY AS A FUNCTION OF SUBSTRATE TEMPERATURE FOR A SERIES OF p-i-n CELLS MADE IN A dc(P) DISCHARGE SYSTEM

the substrate temperature is not a strong variable in this temperature range. Earlier work had shown that the optimum substrate temperature range was ∿210° to 250°C for p-i-n devices made in an rf discharge system [2].

Thus, while the substrate temperature is not a strong variable, the optimum range appears to depend on other deposition conditions.

5.5.4 Optimization of the n-Layer

For p-i-n structures deposited on stainless steel (see Fig. 5-8), a series of devices were made with varying thicknesses of the n-layer. The doping levels for the n- and p-layers were $PH_3/SiH_4 = 4x10^{-2}$ and $B_2H_6/SiH_4 = 1.4x10^{-2}$, respectively. The discharge pressure was 0.63 Torr, and the flow rate was 50 sccm. The substrate temperature was 300°C, and the deposition rate was ∿70 nm/min.

Figure 5-11 shows the variation in V_{oc} and J_{sc} as the thickness of the n-layer is changed, and Fig. 5-12 shows similar data for the fill factor (FF) and the conversion efficiency (η). Clearly, the optimum thickness for the n-layer lies in the range of ∿5 to 10 nm. As the n-layer thickness is increased from zero,

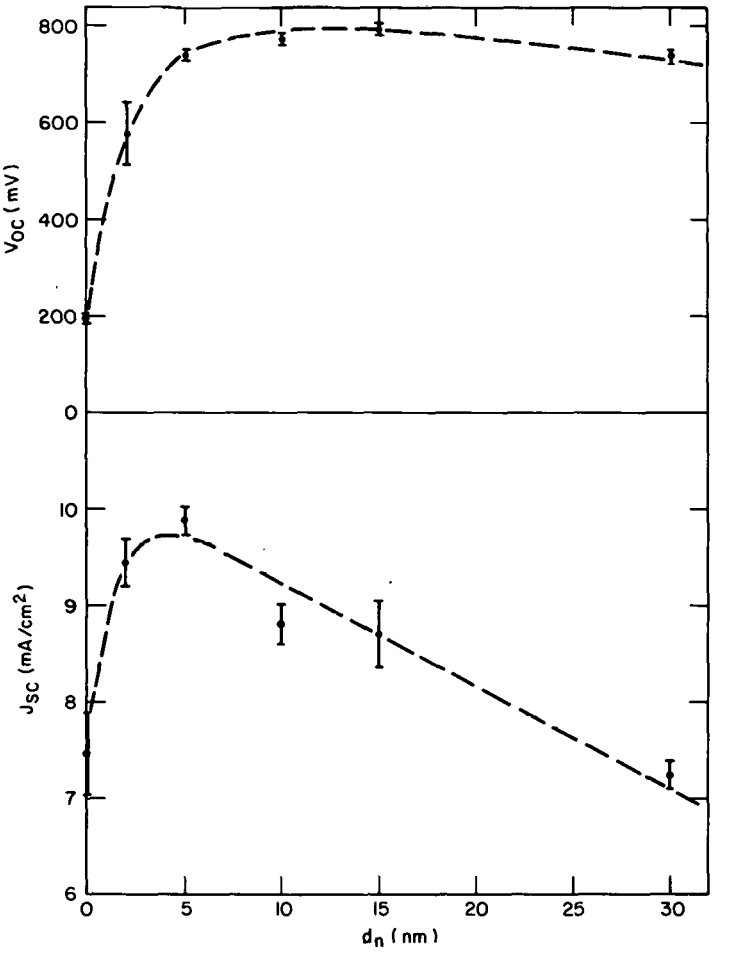

Figure 5-11. V_{oc} AND J_{sc} AS A FUNCTION OF THE THICKNESS OF THE n-LAYER THE ERROR BARS REPRESENT THE STANDARD DEVIATION FOR 5 CELLS AT EACH THICKNESS

the increase in the built-in potential causes both V_{oc} and J_{sc} to initially increase. However, as the n-layer thickness increases beyond ~5 nm, J_{sc} decreases as a result of recombination losses in the n-layer [41].

Another series of devices were made with varying concentrations of PH_3 in the discharge atmosphere (when depositing the top n-layer). Figure 5-13 shows how the conversion efficiency (η) and the fill factor (FF) varied with the ratio PH_3/SiH_4. The optimum doping level for an n-layer ~10 nm thick is $PH_3/SiH_4 \simeq 0.01$ to 0.02. The variation in the fill factor is probably caused by changes in the contact resistance to the ITO since the conductivity of phosphorus-doped a-Si:H maximizes at $PH_3/SiH_4 \simeq 0.01$ to 0.02 [43]. Both V_{oc}

43. N. E. Spear and P. G. LeComber, Solid State Commun. 17, 1193 (1975).

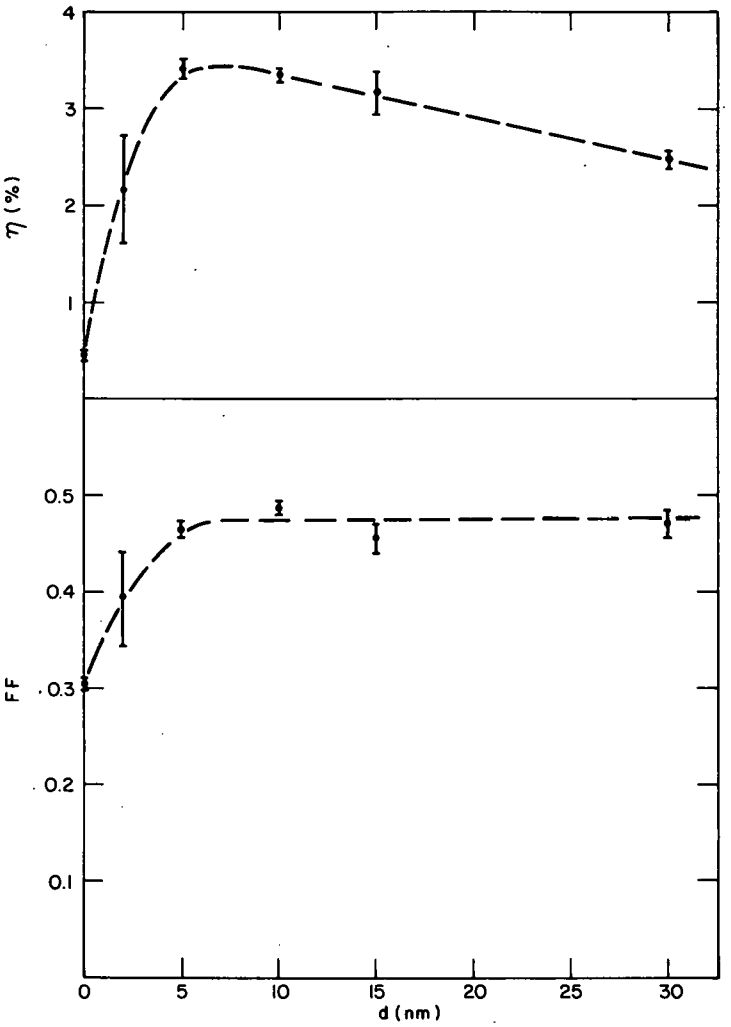

Figure 5-12. FF AND η AS A FUNCTION OF THE THICKNESS OF THE n-LAYER. THE ERROR BARS REPRESENT THE STANDARD DEVIATION FOR 5 CELLS AT EACH THICKNESS

and J_{sc} exhibited only weak dependence on the doping level (except for no n-layer, $PH_3/SiH_4 = 0$) (See Fig. 5-11.)

5.5.5 Optimization of the i-Layer Thickness

The thickness of the i-layer or undoped layer was optimized in another series of experiments, and as shown in Fig. 5-14, the optimum value is ∿0.5 μm. A somewhat larger value (∿0.8 μm) was determined for p-i-n cells made in an rf discharge system and illuminated through the p-layer [41]. The discrepancy may be due to differences in the quality of the undoped a-Si:H layers. However, since hole mobilities are less than those of electron [22], one might expect a shorter collection region for cells illuminated through the n-layer since the holes generated near the front surface must traverse the entire undoped layer.

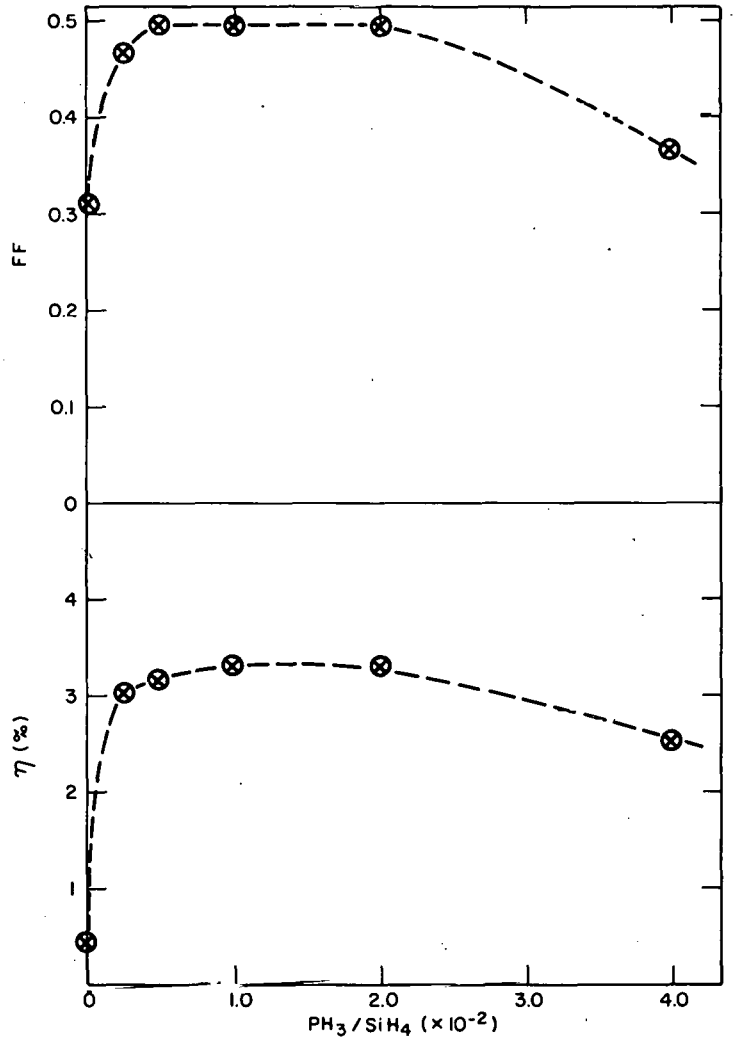

Figure 5-13. FF AND η AS A FUNCTION OF THE DOPING LEVEL, PH_3/SiH_4, ON THE DISCHARGE ATMOSPHERE DURING THE DEPOSITION OF THE n-LAYER

5.5.6 Optimization of the p-Layer

Relatively little change in the performance of p-i-n cells was observed as the doping level for the p-layer (~50 nm thick) was decreased from $B_2H_6/SiH_4 \simeq 1.4\times10^{-2}$ to 5×10^{-3}. However, a further reduction to $B_2H_6/SiH_4 \simeq 1.4\times10^{-3}$ caused a significant decrease in the fill factor.

In another series of experiments, the thickness of the p-layer was varied from zero (no p-layer) to 35 nm (see Fig. 5-15). The performance was roughly constant for thicknesses greater than ~5 nm ($B_2H_6/SiH_4 \simeq 1.4\times10^{-2}$). Surprisingly, relatively good performance ($\eta \simeq 3.65\%$) was obtained without a p-layer; i.e., the undoped layer deposited directly onto the steel substrate.

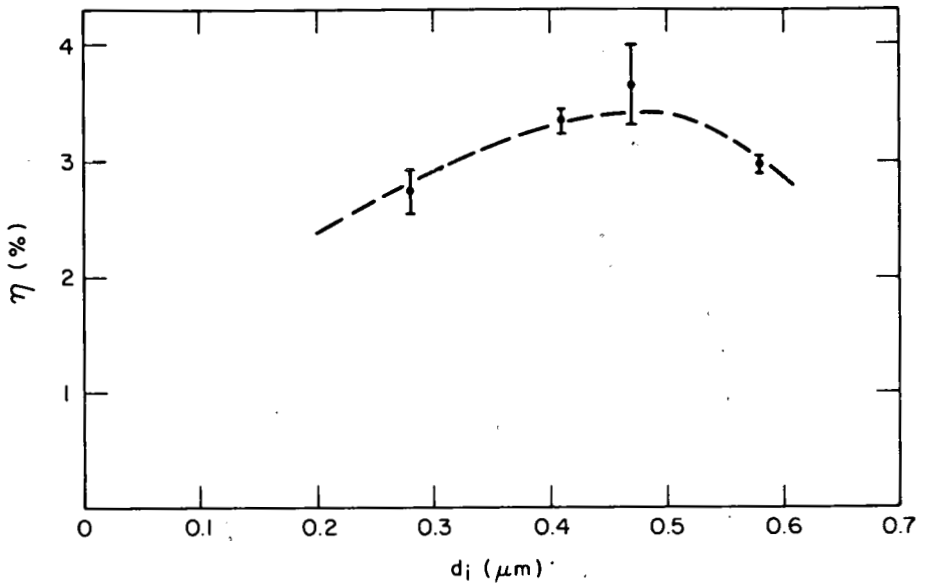

Figure 5-14. CONVERSION EFFICIENCY AS A FUNCTION OF THE i-LAYER THICKNESS. THE ERROR BARS REPRESENT THE STANDARD DEVIATION IN η FOR 5 CELLS MADE AT EACH THICKNESS

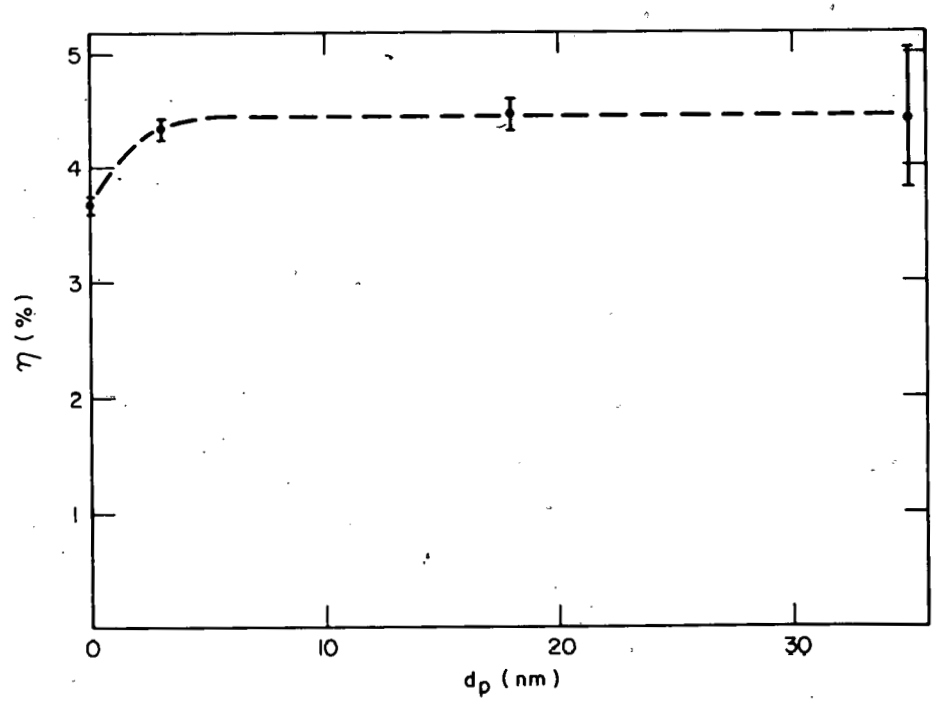

Figure 5-15. CONVERSION EFFICIENCY AS A FUNCTION OF THE p-LAYER THICKNESS. THE ERROR BARS REPRESENT THE STANDARD DEVIATION IN η FOR 5 CELLS MADE AT EACH THICKNESS

The best cell produced to date in these series of optimization experiments had a conversion efficiency of 5.3% ($V_{oc} \simeq 827$ mV, $J_{sc} = 10.9$ mA/cm^2, FF = 0.59, area = 1.19 cm^2).

SECTION 6.0

THEORETICAL AND EXPERIMENTAL EVALUATION OF SOLAR-CELL PARAMETERS

6.1 EFFECT OF LIGHT INTENSITY ON PERFORMANCE

In some cases, the performance of p-i-n cells is limited by the series resistance in the cell circuit. Figure 6-1 shows the I-V characteristics of a p-i-n cell under ∿AM1 illumination, and Fig. 6-2 shows similar data for ∿0.33 AM1 illumination. In the latter case, the current and power are scaled to AM1 so that the results can be easily compared. Lowering the light level by a factor of 3 causes the efficiency to increase from 4.85 to 5.23% mainly as a result of an improvement in the fill factor (0.559 to 0.619).

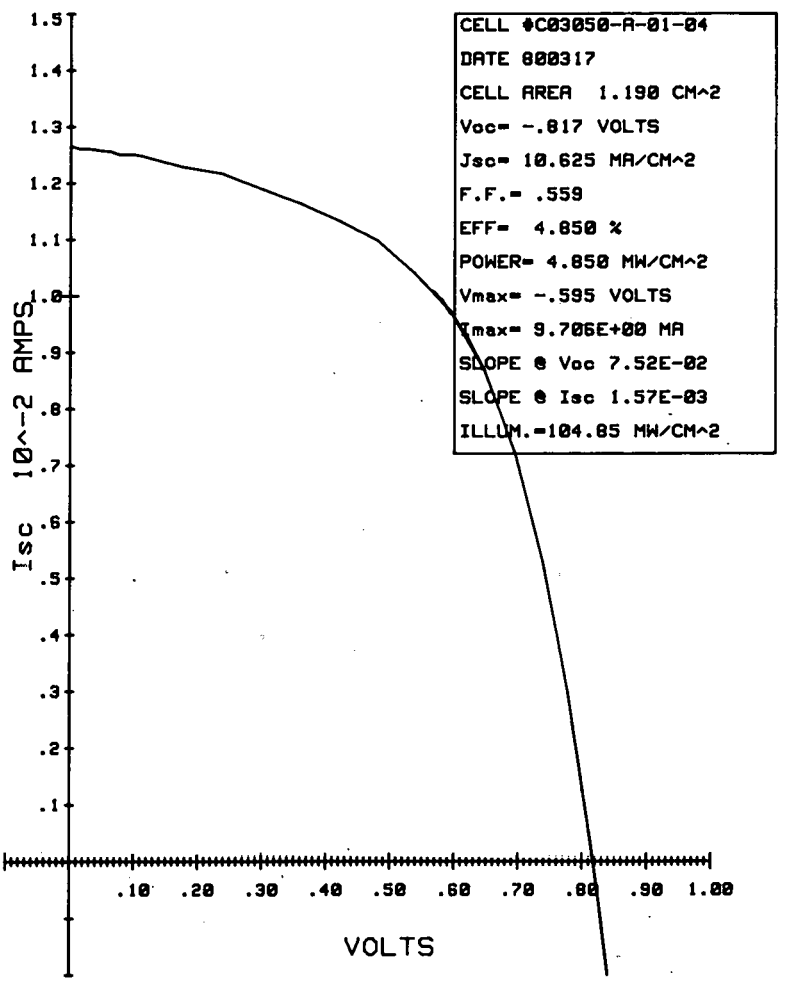

Figure 6-1. I-V CHARACTERISTICS FOR A p-i-n CELL (AREA = 1.19 cm^2) UNDER ∿AM1 ILLUMINATION

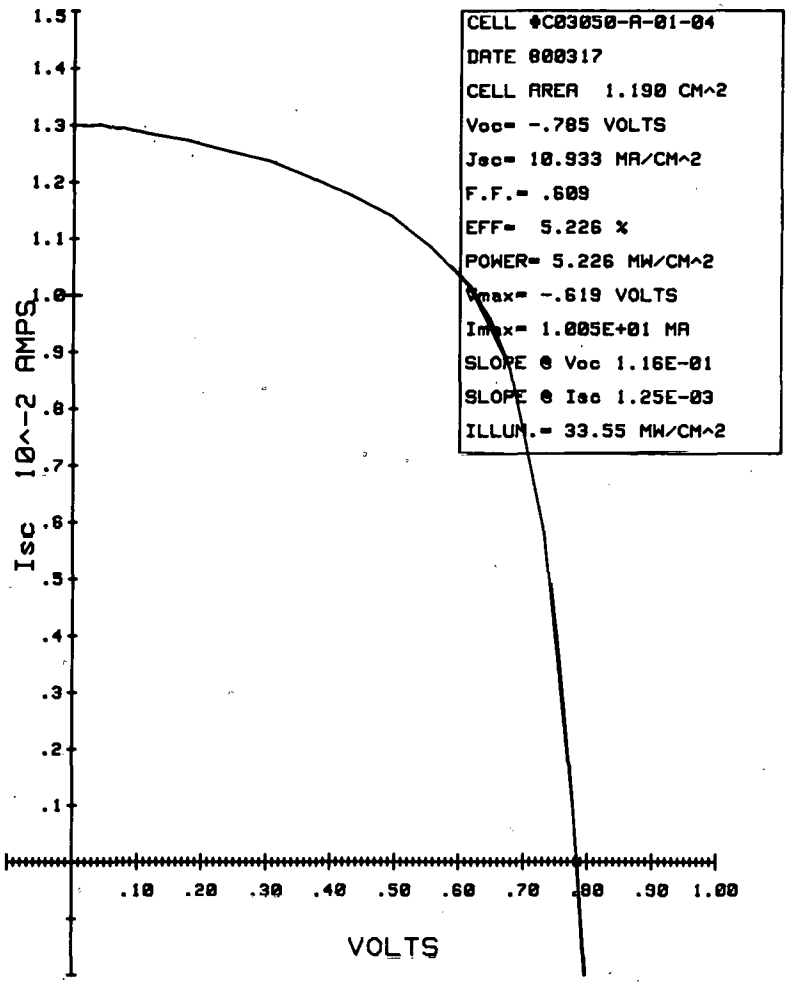

Figure 6-2. I-V CHARACTERISTICS OF A p-i-n CELL UNDER ~0.33 AM1 ILLUMINATION

This cell was limited by a relatively resistive top ITO contact where the sheet resistance was several hundred Ω/□. Lowering the light level reduces the photocurrent and hence, the IR drop in the contacting ITO layer.

6.2 SURFACE PHOTOVOLTAGE PROFILING OF n-i-p AND p-i-n STRUCTURES

In the last Quarterly Report [41] we discussed our surface photovoltage (SPV) measurements on oxidized a-Si:H and found that a very complicated situation was present, apparently due to the existence of both free surface states at the SiO_2 surface and interfacial states at the Si-SiO_2 interface. Rather than continue with more detailed measurements in this area, we are choosing to use our SPV techniques to study the n-i-p and p-i-n solar-cell structures which have recently been developed, and which give such promising results. Our SPV

measurements can be readily interpreted in terms of surface potential changes relative to the substrate, and in this way, light-induced changes in band-bending (i.e., band-flattening) of the solar-cell structure can be studied. Such band-bending should contain as one component, perhaps the dominant component, the available open-circuit voltage. If we sputter-etch through the structure, we should be able to determine what part of the total open-circuit voltage, from metal substrate to free surface of the structure, is contributed to by each section of the solar-cell layer structure.

Our first measurements, made to test our experimental procedures and capabilities, were performed on an n-i-p structure shown schematically in Fig. 6-3. The structure was determined by SIMS profiling. It was chosen for our initial work because the light-induced band-flattening should produce a negative SPV with reference to the stainless steel substrate and is therefore directly comparable to our earlier work.

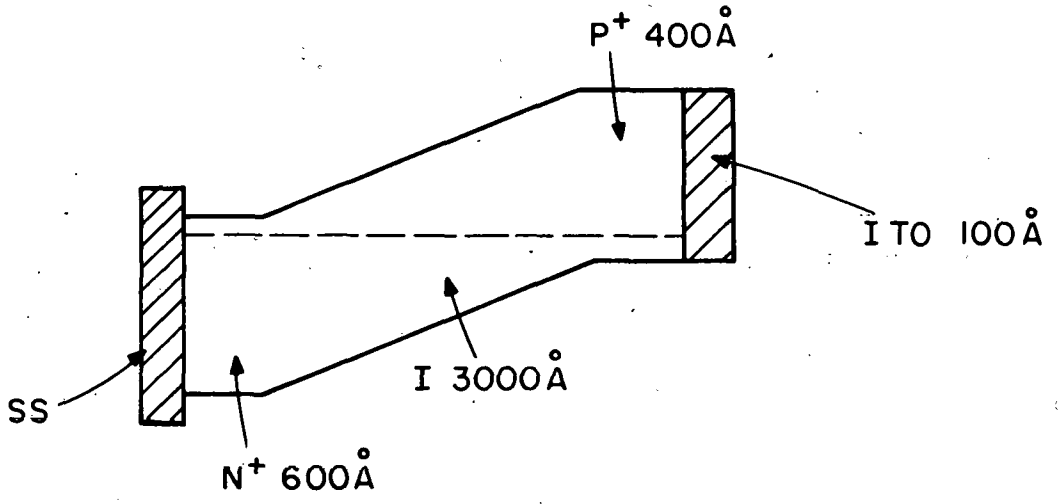

Figure 6-3. SCHEMATIC DRAWING OF p-i-n STRUCTURE ON A STAINLESS STEEL SUBSTRATE WITH AN ITO SEMI-TRANSPARENT TOP CONTACT

The sample (ITO/p-i-n/SS) was mounted in the vacuum system and sputter-cleaned for 1 min, to remove carbon and other contaminants, and then heated for 20 min at 225°C in 10^{-3} Torr oxygen to parallel the customary annealing of the solar-cell structure. (This annealing is primarily for the ITO layer; SIMS analysis has shown that there is no atomic migration during this treatment.) At this

point Auger spectroscopy showed only oxygen, tin, and indium on the surface. The wavelength dependence of both the SPV of this surface and the bulk photoconductivity* of this structure is shown in Fig. 6-4 at room temperature and at -168°C. Isophotonic fluxes were used at each photon energy. Note especially that this photoconductivity is not the photovoltaic current or the short-circuit current of the solar cell; it corresponds to the light-induced change in the volume resistance and results from majority carrier changes. Figure 6-4 shows that the photoconductivity begins at about the optical gap, peaks at 2.2 eV, and then decreases, presumably due to the very strong optical absorption at the higher energies. At room temperature, the SPV (maximum value 575 mV) appears to follow the photoconductivity in threshold and qualitative behavior. This similarity does not extend to -168°C. Here, there seems to be an appreciable contribution to the SPV of about 400 mV due largely to less-than-bandgap response. In addition, there is no decrease in SPV at the higher energies as there is at room temperature. We suggest that these differences may be due to the presence of two components in the SPV. One of these corresponds to the open-circuit voltage of a solar-cell structure, and the other is due to interface states electronically coupled to the valence band at room temperature (hence, producing no net SPV), but isolated from the valence band at -168°C (hence, producing a SPV). We will see in the next paragraph that our light intensity data are completely consistent with this suggestion.

The light intensity behavior of the open-circuit voltage of a solar cell, V_{oc}, is given by the expression

$$V_{oc} = \frac{nkT}{e} \ln \left(\frac{J_{sc}}{J_o} + 1\right) \qquad (6\text{-}1)$$

where n is a number generally between 1 and 2; k, T, and e have their customary meanings; J_{sc} is the short-circuit current, and J_o is the reverse saturation current. J_{sc} varies linearly with light intensity L. Thus, when $\frac{J_{sc}}{J_o} \gg 1$ (i.e., at light intensities) V_{oc} will vary as ln L; when $\frac{J_{sc}}{J_o} \ll 1$ (i.e., at low light levels) V_{oc} will vary as L.

*Measured by using the Auger Spectrometer's electron beam as one contact (see Ref. 2.).

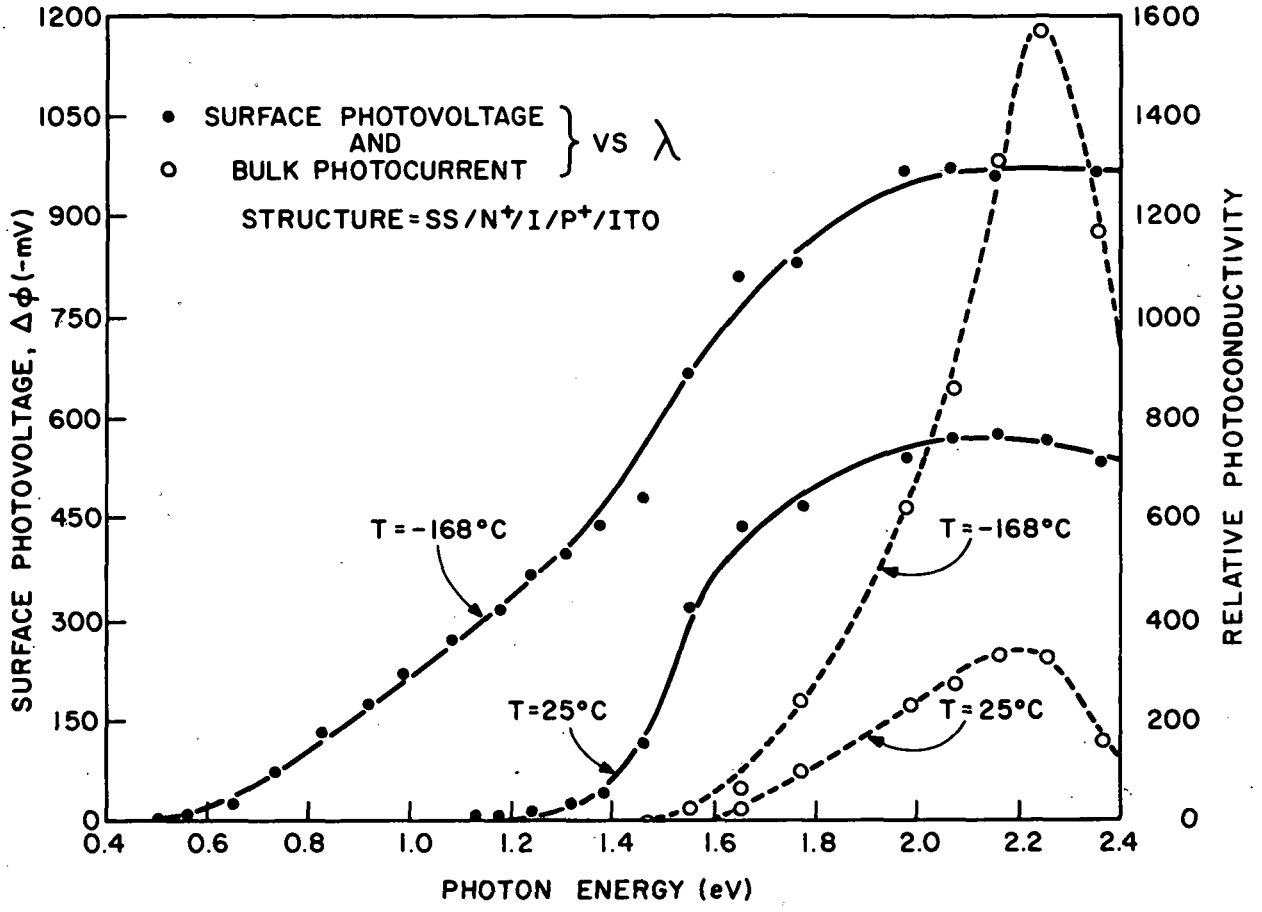

Figure 6-4. SURFACE PHOTOVOLTAGE AND BULK PHOTOCURRENT vs PHOTON ENERGY AT 25°C AND AT -168°C FOR AN ITO/p-i-n STRUCTURE ON STAINLESS STEEL

Figure 6-5 shows the light intensity dependence of the SPV at room temperature and at -168°C for photon energies of 1.77 and 3.1 eV; the significance of these two energies rests in the fact that 1.77-eV light penetrates the entire film with only a 20% reduction in intensity, while 3.1-eV light has a characteristic absorption length (i.e., the reciprocal absorption coefficient) of ~200 Å. The light intensity at 100% has a photon flux of 3×10^{16} photons/cm^2/s. Several features are apparent in Fig. 6-5. At 25°C the SPV response varies linearly with L at low intensities, and with ln L (see inset) at high intensities, with a transition region between the two. In addition, the 3.1-eV response is lower than the 1.77-eV response. The first of these behaviors is exactly that described in Eq. (6-1) for V_{oc}. The second is exactly what is expected for V_{oc} if not all the carriers generated by 3.1 eV are collected,

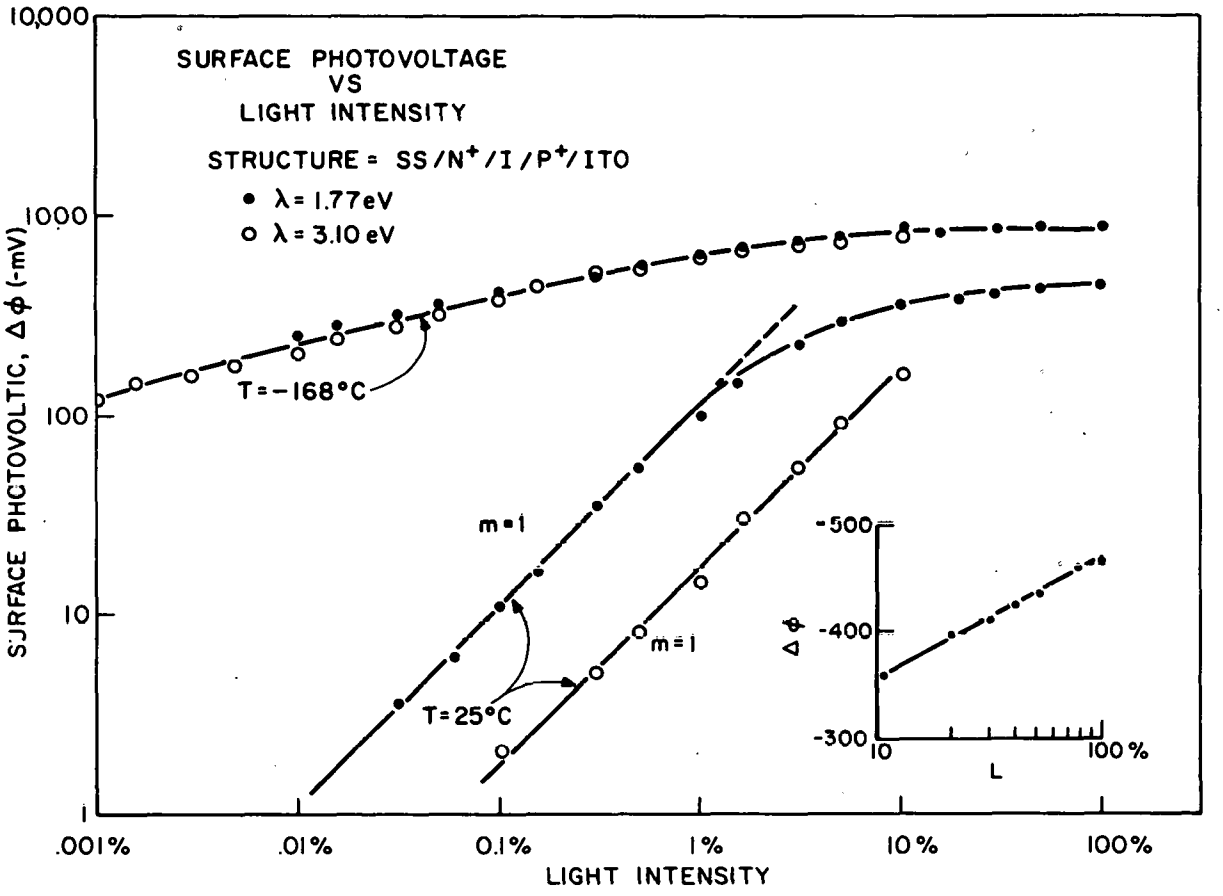

Figure 6-5. INTENSITY DEPENDENCE OF SURFACE PHOTOVOLTAGE AT PHOTON ENERGIES OF 3.1 eV AND 1.77 eV, AND AT TEMPERATURES OF 25°C AND -168°C FOR AN ITO/p-i-n STRUCTURE ON STAINLESS STEEL

something to be expected if the field region (i.e., the space-charge region) does not extend all the way through the i-region, a condition known to exist at room temperature. Consider next the data at T = -168°C, where the 3.1-eV response is the same as the 1.77-eV response. This is not unexpected since at -168°C the "collecting" field does extend throughout the i-region (indicated by earlier work [2]) so that now as many carriers made by 3.1-eV light can be collected as are made by 1.77-eV light. Note also, in Fig. 6-6, that the SPV first saturates, then decreases as ln L, but does not, at lower L, indicate a region of linear variation. This, too, is not unexpected since at -168°C, we would anticipate a much lower value for J_o [see Eq. (6-1)] so that the region where ln L dependence changes to L dependence (i.e., where $\frac{J_{sc}}{J_o} \sim 1$) would occur at much lower intensities. Finally, we can note that the departure from V_{oc} behavior occurs at a SPV value of about 400 mV (L = 0.1), i.e.,

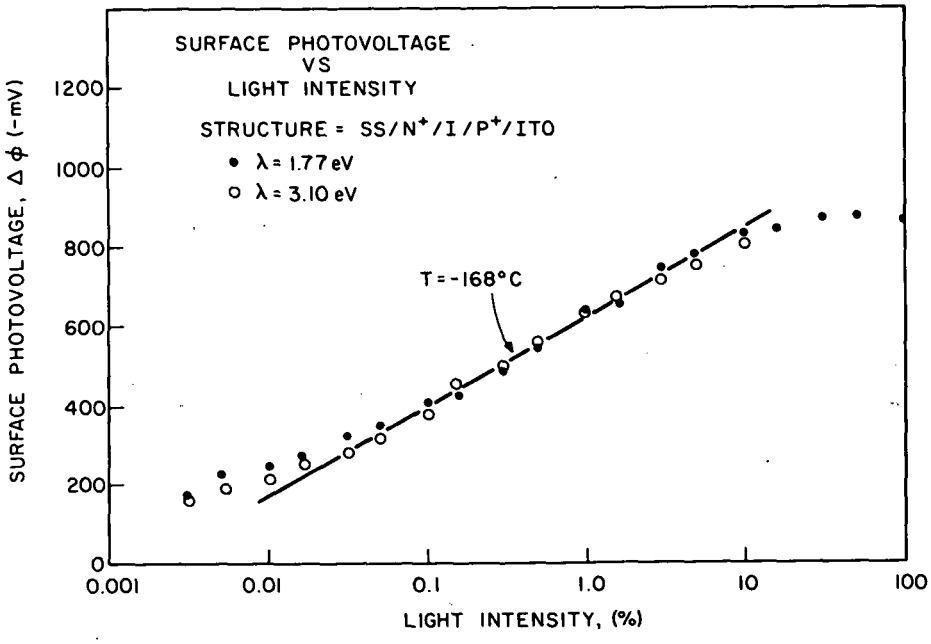

Figure 6-6. SURFACE PHOTOVOLTAGE AT -168°C vs LIGHT INTENSITY FOR AN ITO/p-i-n STRUCTURE

precisely the value suggested by Fig. 6-4 as the contribution made to the total SPV by interfacial states.

In summary, our preliminary work shows that we can successfully analyze many of the properties of the SPV described in Figs. 6-4, 6-5, and 6-6 in terms of the properties of the V_{oc} of the layer structure as a solar cell, plus a SPV component due to interfacial states which contributes at low temperature, but not at room temperature.

The sample was then sputter-etched until all traces of indium and tin were gone from the Auger spectrum and only silicon and a small boron line remained (along with argon, of course). We had sputtered off the ITO layer, exposing the p-type a-Si:H surface. As a result, both the room-temperature and low-temperature maximum SPV were about 200-mV lower than it had been with ITO. We correlate this decrease in SPV with the disappearance of the p-type a-Si:H/ITO interface; i.e., there may be a 200-mV jog in the bands at this interface. Otherwise, both the wavelength dependence and light dependence were qualitatively similar in all major respects to what was found for the ITO surface (Figs. 6-4, 6-5, and 6-6). (One interesting difference was that the crossover point in the intensity curves between ln L dependence and L dependence occurred at lower

intensities, suggesting that the "J_o" for the structure was lower after the ITO had been removed.)

When sufficient sputter-etching is performed, not only to remove the p-layer, but also to take us about 1000 Å into the i-region, further significant changes occur (see Figs. 6-7). That much of the sub-bandgap of the SPV is now caused by surface states is demonstrated by the fact that sputtering the surface reduces the SPV considerably. Sputtering was not a significant factor in the SPV of the p-type a-Si:H or ITO surfaces. Note especially that the threshold at -168°C has shifted to less than 0.5 eV compared to Fig. 6-4; this is consistent with the expected movement of the Fermi level toward the center of the bandgap as we move from the p-region to the i-region. It was also found that as we sputtered into the i-region, the response time for the SPV decay at -168°C increased, which we take to be due to the increased electronic decoupling between bandgap surface states and valence band, i.e., the behavior is approaching more and more that reported for undoped a-Si:H in the Final Report [2].

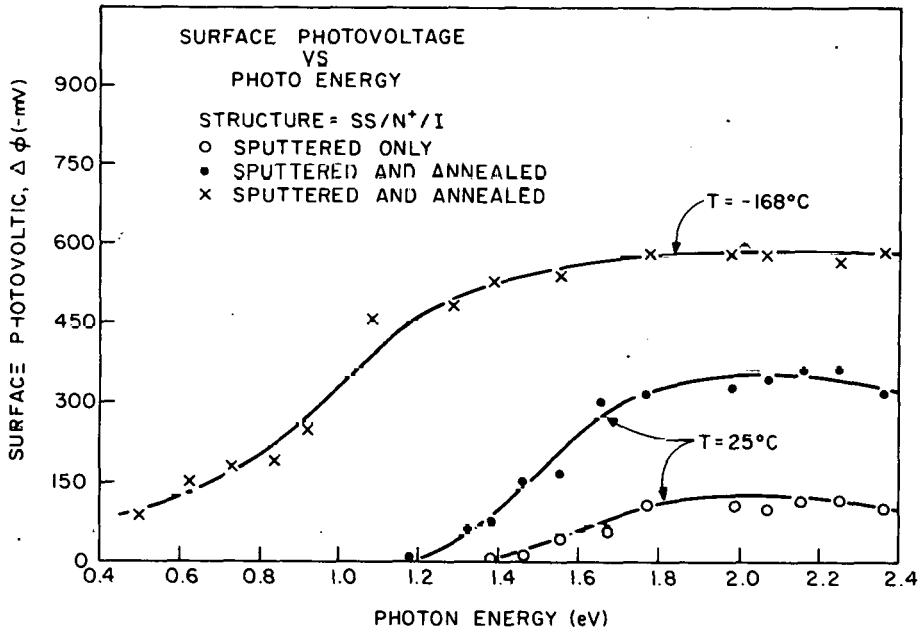

Figure 6-7. SURFACE PHOTOVOLTAGE vs PHOTON ENERGY AT 25°C AND -168°C AFTER ITO AND p-- LAYERS HAVE BEEN SPUTTERED OFF, i.e., AN i-n STRUCTURE

In Fig. 6-8 we show the intensity dependence of the SPV and in the i-region; it is to be compared to that found for the initial ITO surface (Fig. 6-5). Note that now the room-temperature SPV varies linearly with L only at the lowest intensities, while it varies logarithmically over a much greater range of L. At -168°C, saturation with light is much stronger for the I surface. These features can be qualitatively accounted for by a smaller effective J_o for the V_{oc} component of the SPV, and by a larger surface-state component of the SPV.

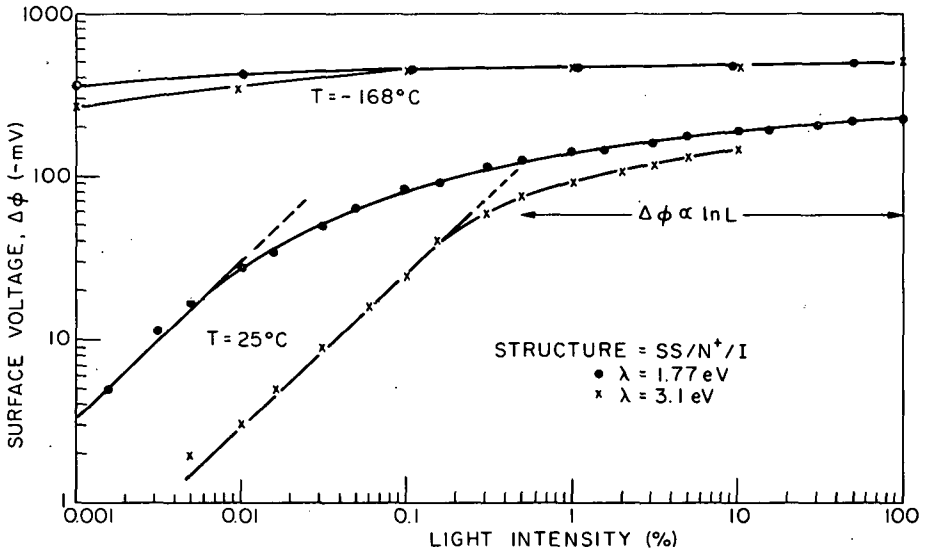

Figure 6-8. SURFACE PHOTOVOLTAGE vs LIGHT INTENSITY AT 25°C AND -168°C FOR THE i-n STRUCTURE

These studies will continue on ITO/n-i-p layers, with attempts to analyze more quantitatively the behavior of the solar-cell parameters in Eq. (6-1).

6.3 STAEBLER-WRONSKI EFFECT

In the Staebler-Wronski (S-W) effect, the dark- and photoconductivity of a-Si:H decreases markedly during exposure to intense light (called "light soaking"). Recently, a controversy has developed as to whether the root cause of this effect stems from bulk changes or surface changes. We are attempting to clarify this issue by measuring surface band-bending directly on appropriate samples which exhibit the S-W effect.

Since one aspect of the surface explanation centers on the interface between the substrate and the a-Si:H, we are making measurements on a-Si:H deposited on a stainless steel substrate and on a quartz substrate. To date, the following observations have been made. The sample on quartz clearly exhibits the S-W effect (only measurements in air have been made so far); the sample on stainless steel does not exhibit the S-W effect. Moreover, the sample on stainless steel does not exhibit the effect with a clean or an oxidized surface in vacuum, nor does it exhibit any light-induced change in band-bending at the free surface (clean, or oxidized). These studies will continue with similar vacuum measurements on quartz samples.

SECTION 7.0

REFERENCES

1. D. E. Carlson, R. S. Crandall, B. Goldstein, J. J. Hanak, A. R. Moore, J. I. Pankove, and D. L. Staebler, Final Report, SAN-1286-8, prepared for Department of Energy under Contract No. EY-C-03-1286, Oct. 1978.
2. D. E. Carlson, I. Balberg, R. S. Crandall, B. Goldstein, J. J. Hanak, J. I. Pankove, D. L. Staebler, H. A. Weakliem, and R. Williams, Final Report, ET/21074-4, prepared for Department of Energy under Contract No. AC03-78-ET-21074, Feb. 1980.
3. T. S. Moss, Photoconductivity in the Elements (Academic Press, New York, 1952).
4. P. G. LeComber, A. Madan, and W. E. Spear, in P. G. LeComber and J. Mort, (eds.) Electronic and Structural Properties of Amorphous Semiconductors (Academic Press, New York, 1973), p. 373.
5. T. Suzuki, M. Hirose, S. Ogose, and Y. Osaka, Phys. Status. Solidi A 42, 337 (1977).
6. P. J. Zanzucchi, C. R. Wronski, and D. E. Carlson, J. App. Phys. 48, 5227 (1977).
7. D. A. Anderson, G. Moddel, R. W. Collins, and W. Paul, paper presented at 8th Int. Conf. Liquid and Amorphous Semiconductors, Cambridge, MA (1979).
8. J. I. Pankove, F. J. Pollack, and C. Schnabolk, ibid.
9. G. D. Cody, B. Abeles, and C. R. Wronski, ibid.
10. R. S. Crandall, J. Non-Cryst. Solids 35 & 36, 38 (1980).
11. A. Rose, RCA Review 12, 362 (1951).
12. R. Williams and R. S. Crandall, RCA Review 40, 371 (1979).
13. K. Hecht, Z. Phys. 77, 235 (1932).
14. R. S. Crandall, R. Williams, and B. E. Tompkins, J. Appl. Phys. 50, 5506 (1979). R. S. Crandall, Appl. Phys. Lett.
15. T. D. Moustakas and K. Weiser, Phys. Rev. B12, 2448 (1975).
16. C. R. Wronski, D. E. Carlson, and R. E. Daniel, Appl. Phys. Lett. 29, 602 (1976).
17. C. R. Wronski, D. E. Carlson, R. E. Daniel, and A. R. Triano, IEDM Technical Digest 75 (1976).
18. D. L. Staebler, Paper Presented at 8th Int. Conf. Liquid and Amorphous Semiconductors, Cambridge, MA, 1979).
19. J. Tauc, Mater. Res. Bull. 5, 721 (1970).
20. W. Fuhs, M. Milleville, and J. Stuke, Phys. Status Solidi (B) 89, 495 (1978).
21. P. G. LeComber and W. E. Spear, Phys. Rev. Lett. 25, 509 (1970).
22. A. R. Moore, Appl. Phys. Lett. 31, 695 (1977).

23. N. F. Mott, and E. A. Davis, Electronic Processes in Non-Crystalline Materials (Clarendon Press, Oxford, England, 1971) p. 238.

24. W. E. Spear and P. G. LeComber, Phil. Mag. 33, 935 (1976); G. H. Dohler, and M. Hirose, in Amorphous and Liquid Semiconductors, edited by W. E. Spear, (G. G. Stevenson Ltd., Dundee, Scotland, 1977) p. 372.

25. B. van Roedern, L. Ley, M. Cardona, and F. W. Smith, Philos. Mag. 13 40, 433 (1979).

26. D. Allan, P. D. LeComber, and W. E. Spear, in Amorphous and Liquid Semiconductors, edited by W. E. Spear, (G. G. Stevenson Ltd., Dundee, Scotland, 1977) p. 323.

27. R. C. Chittick, J. Non-Cryst. Solids 3, 255 (1970).

28. J. I. Pankove, Radiative Recombinations in Semiconductors (Dunod. Paris, France, 1964) p. 201.

29. J. I. Pankove, IEEE J. Quantum Electron. QE4, 119 (1968).

30. A review of both theory and experimental results, with references, can be found in Photo-Magneto-Electric Effect in Semiconductors, O. Garreta and J. Grosvalet, in "Progress in Semiconductors," Vol. 1, (Heywood and Co, 1956) p. 166.

31. A critical review of the theory is given by W. Van Roosbroeck, Phys. Rev. 101, 1713 (1956). The ambipolar concept is emphasized in W. Van Roosbroeck, Phys. Rev. 91, 282, (1953).

32. See also R. A. Smith, Semiconductors (Cambridge University Press, 1959) pp. 214-217.

33. H. S. Sommers, R. E. Berry, and I. Sochard, Phys. Rev. 101, 983 (1956).

34. R. N. Zitter, Phys. Rev. 112, 852 (1958); and R. N. Zitter, A. J. Strauss, and A. E. Attard, Phys. Rev. 115, 266 (1959).

35. See footnote 6 in Ref. 4.

36. T. S. Moss, L. Pincherle, and A. M. Woodward, Proc. Phys. Soc., London, Sect. B 66, 743 (1953).

37. P. G. LeComber, D. I. Jones, and W. E. Spear, Philos. Mag. 35, 1173 (1977).

38. L. Friedman, J. Non-Cryst. Solids 6, 329 (1971).

39. L. Friedman, Philos. Mag. 38, 467 (1978).

40. D. Emin, Philos. Mag. 35, 1189 (1977).

41. D. E. Carlson, R. S. Crandall, J. Dresner, B. Goldstein, J. J. Hanak, A. R. Moore, J. I. Pankove, and H. A. Weakliem, Quarterly Report No. 1, SERI/PR-9-8254-1, prepared for the Solar Energy Research Institute under Subcontract No. XJ-9-8254.

42. C. W. Magee, RCA Laboratories.

43. W. E. Spear and P. G. LeComber, Solid State Commun. 17, 1193 (1975).

*U.S. GOVERNMENT PRINTING OFFICE:1980 740-145/535